Chapter 6

Kinematics of the Particle Flux

6.1 Preamble

Herein we examine essential kinematic elements of the sediment particle flux, with relevance to both hillslope and river systems. In stark contrast to descriptions of transport under ordinary continuum conditions, descriptions of the particle flux and its divergence under rarefied conditions must explicitly refer to the spatial and temporal resolutions involved. This is essential, as definitions of the flux and its divergence are inextricably conditioned on the lengths and time intervals used in averaging. This topic therefore serves as the starting point of this chapter.

We then turn to definitions of the particle flux, focusing on the *activity form* and the *entrainment form* of these definitions. Because these definitions are centered on the movement of particles through a control surface, they are immediately adaptable to descriptions of the Exner equation involving the divergence of the flux. Here we provide a preview of the idea that the particle flux involves both advective and diffusive parts, and the importance of distinguishing between probabilistically expected conditions versus what occurs in any realization due to the relatively small numbers of particles involved in rarefied transport.

We then examine implications and consequences of time averaging. This is focused on measurements of time series of sediment transport, and how the measurement interval Δt influences our understanding and interpretation of the particle flux. This notably includes how averaging over Δt influences the rate of convergence of estimates of the flux to the expected value and the related observation that the variance of the flux systematically varies with the sampling interval, with decided practical implications. Our descriptions of counting processes covered in Chapter 4 have a central role in this topic.

We end the chapter by examining the concepts of *local transport* versus *nonlocal transport*. We clarify the physical versus the mathematical interpretations of these concepts, and why all sediment transport is nonlocal when viewed from a physical perspective at the scale of particle motions.

6.2 Resolution

6.2.1 Temporal Resolution

Regarding notation, in what follows we choose initial conditions at time $t = 0$ such that the time t and the time interval Δt usually are interchangeable. For example, if $N(t)$ denotes a number of particles accumulated at time t with $N(0) = 0$ then likewise $N(\Delta t)$ might denote this number occurring during the interval Δt such that $N(t) = N(\Delta t)$. However, Δt also is intended to represent an interval of time without reference to an initial time, notably an averaging interval. We use $t = T$ to denote a total time, for example, the duration of an experiment.

Consider a cloud of particles moving through a surface A that is oriented normal to the x axis (Figure 6.1). The particles may cross A in both the positive and negative directions. Let us associate

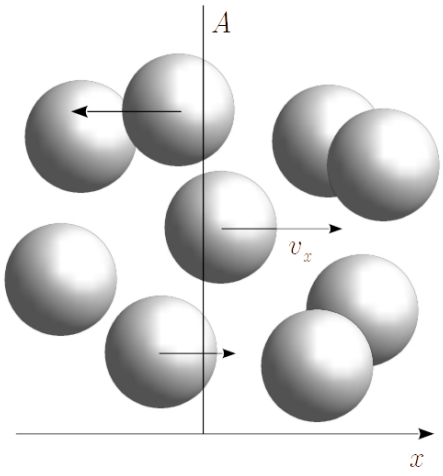

Figure 6.1: Definition diagram showing particles moving through a control surface A with velocity components v_x parallel to x.

the coordinate position of a particle with its center of mass, a point. Then let $I(t;A) = \{\mathrm{sgn}[v_x(t_i)]\delta(t_i)\}$ with $i = 1, 2, 3, ...$ denote a time series of crossing events, where $\delta(t_i)$ denotes an integrable Dirac impulse defined at the instant that a particle point crosses the surface A and $v_x(t_i)$ denotes the associated particle velocity component parallel to x. Here the use of $\mathrm{sgn}[v_x(t_i)]$ is merely to allow for crossings in the positive and negative directions. The appearance of A after the semicolon reminds us that the time series is specific to the area A, a point that we elaborate below.[1]

Whether viewed at the atomistic scale of a continuum fluid or at the sediment particle scale, the cumulative number of indistinguishable particles crossing A during an interval $(0, t]$ is

$$N(t;A) = \int_0^t I(t';A)\,\mathrm{d}t' \,. \tag{6.1}$$

The number $N(t;A)$ is a discontinuous stepped function whose local derivative with respect to time is either zero or undefined. More generally, the cumulative number of particles crossing A during an interval $(t, t+\Delta t]$ is

$$N(\Delta t;A) = \int_t^{t+\Delta t} I(t';A)\,\mathrm{d}t' \,. \tag{6.2}$$

The particle number flux associated with this interval is then defined as

$$q_{nx}(\Delta t;A) = \frac{N(\Delta t;A)}{A\Delta t} \,. \tag{6.3}$$

In the specific case of two-dimensional transport over a surface, as with rain splash and bed load transport, the vertically integrated number flux parallel to x is

$$q_{nx}(\Delta t;\Delta y) = \frac{1}{\Delta y \Delta t}\int_t^{t+\Delta t} I(t';\Delta y)\,\mathrm{d}t' \,, \tag{6.4}$$

[1] K. Pierce (personal communication, 2023) points out that one can alternatively write $I(t;A)$ in terms of a sum over all particles and possible starting positions using $\mathrm{sgn}[v_x(\tau_i)]\delta(t-\tau_i)$, where τ_i denotes the crossing time of the ith particle.

and the number flux parallel to y is

$$q_{ny}(\Delta t;\Delta x) = \frac{1}{\Delta x \Delta t}\int_t^{t+\Delta t} I(t';\Delta x)\,\mathrm{d}t' \,. \tag{6.5}$$

Multiplying these expressions by the particle volume V_p gives the particle volumetric flux components $q_x(\Delta t) = V_\mathrm{p} q_{nx}$ and $q_y(\Delta t) = V_\mathrm{p} q_{ny}$. In these definitions of the volumetric flux the temporal resolution is no shorter than $T_D \sim D/\langle v_x\rangle$ and $T_D \sim D/\langle v_y\rangle$, where $\langle v_x\rangle$ and $\langle v_y\rangle$ are ensemble averaged particle velocities defined for the specific process and series I (see below). These are the typical times required for a particle with diameter D to cross A, Δy or Δx. These definitions of the flux are effectively the same as those examined by Pierce et al. (2022) and used by Ma et al. (2014), Ancey and Pascal (2020) and Li et al. (2023).

Here is a particularly important sidebar regarding notation and perceptions. Choosing (6.4) for illustration, the flux q_{nx} — a random variable — is by definition a time average of the time series I, that is, an average over the interval Δt. One might therefore be tempted to emphasize this point by writing $\overline{q_{nx}}$. However, in writing $\overline{q_{nx}}$ there is the risk of misinterpreting this as implying that q_{nx} is defined as an instantaneous quantity in the sense of a time-continuous function, such that $\overline{q_{nx}}$ denotes its time average. But in fact q_{nx} *cannot* be interpreted as an instantaneous quantity in this manner. It is equal to zero in the limit of $\Delta t \to 0$. When we denote the flux as q_{nx}, this by definition involves a time average of the time series I. If one wishes to emphasize the time averaging, then we can do this by writing $q_{nx}(\Delta t;\Delta y)\Delta y = \overline{I(t;\Delta y)}$, where now the overline represents the integration and division by Δt in (6.4). Below we show how the flux q_{nx} is related to the idea of a moving average.

The definitions above are generic, without reference to the specific stochastic structure of the time series I. There are numerous possibilities. For example, with $\mathrm{sgn}[v_x(t_i)] = 1$ for all t_i, then I might be a Poisson process or a mixture of Poisson processes. For example, we show in Chapter 12 that the crossings of the largest particles in a gravel mixture transported as bed load are well approximated by a Poisson process, whereas the series I for smaller particles exhibit overdispersion reflecting unsteady conditions and varying forms of intermittency. The stochastic formulation of bed load transport by Ancey et al. (2008) treats entrainment and deposition within a control volume as Markov birth–death processes whence effects of collective entrainment (Ancey et al., 2008; Lee and Jerolmack, 2018) lead to a description of the particle flux as a Cox process (Ma et al., 2014), essentially an inhomogeneous Poisson process in which the Poisson rate is itself a stochastic process. The time series I might be a Lévy process consisting of the difference of two Poisson processes or compound Poisson processes. For example, we show in Chapter 11 that the particle flux due to rain splash is a Lévy process consisting of opposing (downslope and upslope) compound Poisson processes. And, if crossing events are reinterpreted as raindrop impacts leading to rain splash transport, then the time series I is a Poisson process and the number of particles entrained by impacts is a compound Poisson process. Similarly, if crossing events are reinterpreted as bed load particle entrainment events, then in the simplest case the time series I may be treated as a Poisson process (Einstein, 1950). We add details regarding the stochastic structure of I as needed in later sections with reference to related work (e.g. Einstein, 1950; Uijlenhoet et al., 1999; Smith et al., 2009; Heyman et al., 2013; Ancey and Heyman, 2014; Ma et al., 2014; Pierce et al., 2022). Meanwhile, because of its simplicity and intuitive clarity, here we follow Ancey and Pascal (2020) and Furbish and Doane (2021) and appeal to a homogeneous Poisson process to illustrate key points related to temporal resolution.

With $\mathrm{sgn}[v_x(t_i)] = 1$ for all t_i, consider a set of realizations of the number $N(t)$ and the flux $q_{nx}(\Delta t)$ generated from a Poisson process with fixed intensity λ (Figure 6.2). In this example the number $N(t)$ at time t is described by a Poisson distribution with expected value $\mathrm{E}[N(t)] = \langle N(t)\rangle = \lambda t$ and variance $\mathrm{Var}[N(t)] = \lambda t$. That is, the variance increases linearly and thus indefinitely with time. The standard deviation of the flux $q_{nx}(\Delta t)$ is $\sqrt{\lambda/\Delta t}$ and the coefficient of variation is $1/\sqrt{\lambda\Delta t}$; thus both decay as $(\Delta t)^{-1/2}$. Note that the specific examples concerning rain splash and bed load transport mentioned

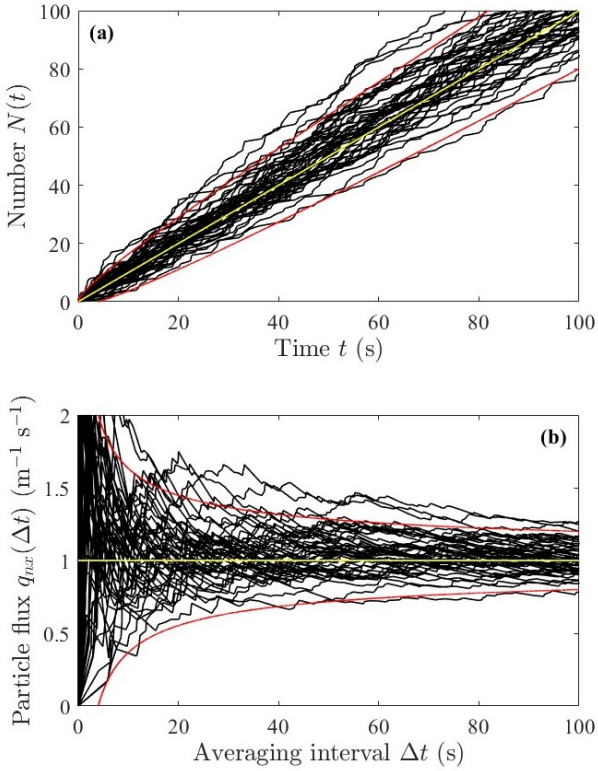

Figure 6.2: Plot of (top) 50 realizations (black lines) of particle number $N(t)$ versus time t showing increasing variance with t about expected value (yellow line) and ± 2 standard deviations (red lines); and (bottom) 50 realizations (black lines) of time-averaged particle number flux q_{nx} versus averaging interval Δt showing convergence to ensemble expected value $\langle q_{nx} \rangle$ (yellow line) with ± 2 standard deviations (red lines). Plots are generated with Poisson rate $\lambda = \langle q_{nx} \rangle \Delta y = 1$ s^{-1}. Adapted from Furbish and Doane (2021).

above, although not necessarily described as Poisson processes, nonetheless share these well-known qualities: the variance of the number of particle crossings $N(t)$ grows indefinitely with time t, and the standard deviation and coefficient of variation of the associated flux $q_{nx}(\Delta t)$ decay inversely with the averaging interval as $(\Delta t)^{-1/2}$. (This is not necessarily the case for inhomogeneous series; see Section 6.4.1.)

It is essential to appreciate that $N(t)$, $q_{nx}(\Delta t)$ and $q_{ny}(\Delta t)$ are random variables, not deterministic quantities (e.g. Ancey, 2010; Ancey and Heyman, 2014; Ma et al., 2014; Ancey and Pascal, 2020; Furbish and Doane, 2021; Pierce, 2021; Pierce et al., 2022). If $I(t; A)$, $I(t; \Delta y)$ or $I(t; \Delta x)$ is statistically homogeneous (as with a homogeneous Poisson process; Figure 6.2), then strictly speaking the fluxes in (6.3), (6.4) and (6.5) converge to ensemble expected values only in the limit of $\Delta t \to \infty$, assuming this limit exists. For a finite interval Δt these expressions therefore represent estimates of the expected values, $\langle q_{nx} \rangle$ and $\langle q_{ny} \rangle$, with associated uncertainty, and this uncertainty decreases as Δt increases. This is at the heart of item (1) in Section 1.3.2, that the law of large numbers yields convergence to ensemble values for fluid systems but not necessarily for sediment systems. For example, as elaborated in Appendix A, with air at ordinary temperature-pressure conditions at a resolution of $A = 10^{-6}$ m^2 the particle flux converges rapidly to a value with negligible uncertainty within $\Delta t = 10^{-6}$ s; this time decreases with coarser spatial resolution. In stark contrast, with rain splash and bed load transport, convergence of the particle flux to a value with small uncertainty may require many minutes to hours or more depending on the spatial resolution and the intensity of particle excitation (Figures 1.1 and

1.2). In the case of an inhomogeneous process, for example, the particle flux associated with rain splash during unsteady rainfall, convergence generally does not occur (Chapter 11).

The fluxes given by (6.3), (6.4) and (6.5) lead to two key points. First, the temporal resolution of the flux generally is not independent of the spatial resolution. For given transport conditions the expected (average) rate of the impulses composing the time series $I(t;\Delta y)$ or $I(t;\Delta x)$ generally varies with the lengths Δy and Δx (e.g. Furbish and Doane, 2021; Williams and Furbish, 2021; also see Section 6.3). For example, with aerially uniform, steady transport (e.g. rain splash or bed load) the number of crossing events on average increases with the products Δyt and Δxt. And if the time series is Poisson or Poisson-like such that for all events $\mathrm{sgn}[v_x(t_i)] = \mathrm{sgn}[v_y(t_i)] = 1$ then $N(t)$ increases monotonically with the products Δyt and Δxt. Thus, the uncertainty of the calculated average, (6.4) and (6.5), decreases with increasing time Δt or increasing lengths Δy and Δx, or both. In addition, we must not imagine that the flux at a coordinate position (x, y) is obtained by taking the limits of (6.4) and (6.5) as $\Delta y \rightarrow 0$ and $\Delta x \rightarrow 0$. This is not intended. (Indeed, these limits are zero.) Instead, as elaborated below, Δy and Δx provide the scale of resolution analogues to a continuum physical point.

Second, such noise-driven systems can confound experimental estimates of time-averaged transport rates (e.g. Ancey et al., 2015; Ancey and Pascal, 2020; Ancey and Recking, 2023) owing to the finite duration of experimental measurements. We reinforce this point below (Section 6.4.1) and in Chapter 12 in relation to bed load transport of a mixture of particle sizes, where we note that (6.4) is the basis of measurements of the bed load sediment flux at the end of an experimental flume with width Δy. A key outcome is that we can never know the "true" underlying rate of a Poisson process (or similar stochastic processes) based on experimental measurements, as described in Chapter 4.

Because (6.3), (6.4) and (6.5) simply involve the counting of particles that cross a coordinate position — a counting process — these expressions represent the most basic, unambiguous definitions of the flux possible. These expressions contain no information about particle kinematics, for example, particle velocities, displacements or travel times, and such quantities cannot be derived from these expressions. Yet definitions of the flux that involve such kinematic quantities must be consistent with (6.3), (6.4) and (6.5). We elaborate this point in Section 6.3 following a brief consideration of spatial resolution.

6.2.2 Spatial Resolution

Consider a Cartesian xyz coordinate system. The x axis is positive in the downstream or downslope direction, the horizontal y axis is positive toward the left when looking downstream or downslope, and the z axis is positive upward. Let $z = \eta(\mathbf{x}, t)$ denote the elevation of the streambed or land surface at coordinate position $\mathbf{x} = (x, y)$ with volumetric particle concentration c_b. Now, with respect to bed load transport or transport by rain splash, for example, we are accustomed to seeing the divergence form of the two-dimensional Exner equation written as

$$c_\mathrm{b}\frac{\partial \eta(\mathbf{x},t)}{\partial t} = -\nabla \cdot \mathbf{q}(\mathbf{x},t)\,, \tag{6.6}$$

where $\nabla = \mathbf{i}\partial/\partial x + \mathbf{j}\partial/\partial y$ and the vertically integrated particle volumetric flux $\mathbf{q} = \mathbf{i}q_x + \mathbf{j}q_x$ with components $q_x(\mathbf{x}, t)$ and $q_y(\mathbf{x}, t)$ parallel to x and y.[2] In order to make an important comparison below, the one-dimensional version of (6.6) parallel to x is

$$c_\mathrm{b}\frac{\partial \eta(x,t)}{\partial t} = -\frac{\partial q_x(x,t)}{\partial x}\,. \tag{6.7}$$

[2]As described in Chapter 7, this form of the Exner equation assumes the local particle activity is steady, or that moving particles within any control area $\Delta x \Delta y$ are included in the calculation of the elevation $\eta(\mathbf{x}, t)$ (Furbish et al., 2012a).

In these local Eulerian expressions the streambed or land-surface elevation η and the component fluxes q_x and q_y are continuously differentiable functions with respect to position $\mathbf{x}$ and time t. Moreover, as written the component fluxes q_x and q_y are deterministic quantities.

Momentarily setting aside our conclusions from the preceding section, the expressions (6.6) and (6.7) have the form that we normally associate with ordinary continuum materials. If we say that continuum conditions exist, thereby justifying the continuously differentiable forms of (6.6) and (6.7), then we must in turn demonstrate that we are justified in treating the component fluxes $q_x(\mathbf{x}, t)$ and $q_y(\mathbf{x}, t)$ as deterministic quantities. If we do not claim that continuum conditions exist, then we must clarify what (6.6) and (6.7) actually represent. The local term on the left side of (6.6) and (6.7) is essentially kinematic. The physics represented by these expressions in relation to the presence or absence of continuum conditions is contained in the fluxes, and this is what we focus on.

In appealing to the one-dimensional expression (6.7), and momentarily focusing on bed load transport, there is no reference to the transverse dimension of the problem. In practice we might claim that the flux $q_x(x, t)$ refers to a specific transverse dimension, for example, the width Y of an experimental flume or a river. In this situation $q_x(x, t)$ is informally width averaged. Likewise the elevation $\eta(x, t)$ is informally width averaged. Momentarily neglecting the question of functional smoothness with respect to time, if the flux $q_x(x, t)$ is a deterministic quantity that satisfies the continuum hypothesis, then in principle its magnitude varies smoothly with y at a scale $\Delta y < Y$ consistent with the averaging provided by a physical point (a representative elementary volume) as defined in continuum mechanics. If, on the other hand, we concede that the flux q_x does not vary smoothly with y, but instead is just a width-averaged quantity, then we need to be prepared to offer a similar interpretation of the flux $q_y(\mathbf{x}, t)$ as used in the two-dimensional expression (6.6). Namely, if $q_x(\mathbf{x}, t)$ is to be considered a flux that is averaged with respect to a specific length $\Delta y \leq Y$ normal to x, then what is the specific length Δx normal to y that is to be used to define the flux $q_y(\mathbf{x}, t)$? As Coleman and Nikora (2009) note, the choice of these length scales bears on the interpretation of sediment attributes and transport, yet it is unusual to see explicit attention to this matter.

The answer to the question above is not necessarily as simple as choosing a length $\Delta x = \Delta y \leq Y$. As described in the previous section, the time convergence of the flux to a value that we might view as being a deterministic quantity fundamentally depends on the lengths Δx and Δy. With reference to item (3) in Section 1.3.2, we show in later chapters that the strongly unidirectional (anisotropic) motions of bed load particles might require that $\Delta x \gg \Delta y$ to achieve comparable estimates of the component fluxes for a specified averaging interval Δt, whereas the radial trajectories of particles during rain splash lead to comparable estimates with $\Delta x \approx \Delta y$. Moreover, if for a specified precision and averaging interval Δt the defining lengths Δx and Δy approach the size of the flume width or river width, or the size of streambed features to which we are applying (6.6) and (6.7) — for example, ripples, dunes or bars — then (6.6) and (6.7) are in fact not local expressions of conservation as we normally envision and apply them. Indeed, we show in later chapters why a continuum-like formulation cannot describe effects of nonlocal transport (e.g. Doane, 2018; Doane et al., 2018, 2019; Furbish et al., 2021a; Furbish and Doane, 2021) in approaching the scale of particle motions.

As written, (6.6) and (6.7) are therefore entirely misleading. We must in fact recast these in terms of ensemble expected conditions that explicitly acknowledge the spatial resolution involved in any particular problem, owing to the fact that rarefied conditions do not admit a continuum-like description. For example, as described in later chapters one possibility is to rewrite (6.7) as

$$c_{\mathrm{b}} \frac{\partial \langle \eta(x,t) \rangle}{\partial t} \Delta x \Delta y = -\lambda_E + \lambda_D \, . \tag{6.8}$$

Here the elevation $\langle \eta(x, t) \rangle$ is explicitly averaged over a specified area $\Delta x \Delta y$ that defines the spatial resolution of the problem. The quantity λ_D [L^3 T^{-1}] is the rate (a Poisson-like intensity) of deposition within $\Delta x \Delta y$, and λ_E [L^3 T^{-1}] is the rate of entrainment *with emigration* from $\Delta x \Delta y$, where the added

emphasis highlights that particles entrained within $\Delta x \Delta y$ do not necessarily leave this area. Moreover, these quantities must reflect the divergence implied by the right side of (6.7). To be clear, (6.8) does *not* describe what occurs in any realization. Rather, this describes the probabilistically expected behavior. Individual realizations are determined by the specific stochastic structure of the processes represented by λ_E and λ_D, and such realizations involve fluctuations in the numbers of particles entering and leaving the area $\Delta x \Delta y$ giving fluctuations in the elevation $\eta(x,t)$ about the expected value $\langle \eta(x,t) \rangle$.

6.3 Descriptions of the Flux

There are several definitions of the particle flux, notably in relation to bed load transport (e.g. Einstein, 1950; Tsujimoto, 1978; Nakagawa and Tsujimoto, 1980; Ballio et al., 2014, 2018; Ancey, 2010; Furbish et al., 2012a, 2017a). Here we focus on two definitions that are centered on the movement of particle motions through a control surface. The *activity form* is continuum-like in its conceptualization, and the *entrainment form* is centered on describing particle motions over a sediment surface in relation to entrainment and disentrainment.

6.3.1 Activity Form

Here we initially focus on the particle volumetric flux, then translate the results to the particle number flux in relation to the definitions in Section 6.2.1.[3] Recall that in Chapter 1 we introduced a precise definition of the volumetric flux associated with a control surface A,

$$q_x(t) = \frac{1}{A} \int_A \mathbf{u} \cdot \mathbf{n} \, \mathrm{d}A \, , \tag{6.9}$$

where $\mathbf{u}$ is the discontinuous particle velocity field viewed at the surface A, and $\mathbf{n}$ is the unit vector normal to A. We noted that this definition is impractical, and that conventional descriptions instead appeal to averaged quantities, the average particle velocity and number concentration, to replace the detailed information contained in the particle velocity field $\mathbf{u}$ at the surface A. This strategy is central in defining the activity form of the flux, which is continuum-like in its conceptualization.

We start with a discrete version of (6.9) to reveal details of particle shape and motion that figure into this deterministic definition of the flux. This provides the basis for illustrating that, in appealing to averaged particle quantities (specifically the mean particle velocity and concentration) to replace the detailed information embodied in (6.9), the resulting description of the flux must in general involve both advective and diffusive parts. We start with a rendering of the geometry and motion of a single particle.

Consider a particle with diameter D [L] that is moving parallel to x through a surface A positioned at $x = 0$ (Figure 6.3). Let ξ_i [L] denote the position of the nose of the particle relative to $x = 0$, and let $V_i(\xi_i)$ [L^3] denote the volume of the particle that is to the right of $x = 0$ as a function of ξ_i. The particle volume discharge $Q_i(t)$ across A is (Appendix D)

$$Q_i(t) = S_i(\xi_i) u_{xi} \, , \tag{6.10}$$

where $S_i(\xi_i) = \partial V_i / \partial \xi_i$ [L^2] is like a hypsometric function of the particle, equal to its cross-sectional area on the surface A at $x = 0$, and $u_{xi} = \mathrm{d}\xi_i / \mathrm{d}t$ [$\mathrm{L\ T}^{-1}$] is its velocity parallel to x.

Consider, then, a cloud of equal-sized particles which are moving with varying velocities parallel to x toward and through a surface A of width Δy positioned at $x = 0$ (Figure 6.3). Let $N(t)$ denote

[3] Much of the material in this section and Appendix D comes from Furbish et al. (2012a).

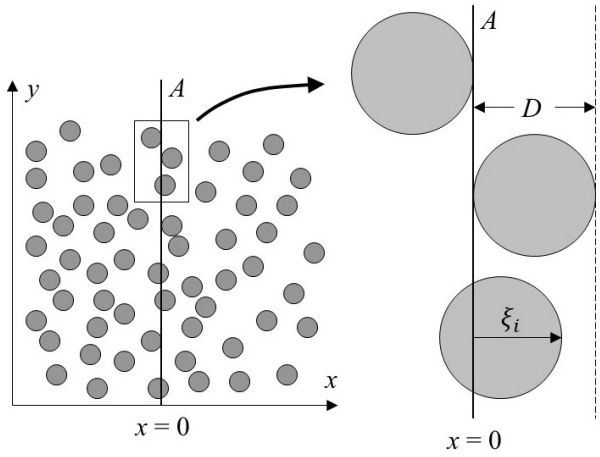

Figure 6.3: Definition diagram showing cloud of particles moving with varying velocities parallel to x toward and through a control surface A positioned at $x = 0$, where ξ_i denotes the distance that the nose of the ith particle is relative to $x = 0$.

the number of particles intersecting A at time t. If ξ_i denotes the distance between the nose of the ith particle and $x = 0$, then the instantaneous volumetric flux q_x across A is

$$q_x(t) = \frac{1}{\Delta y}\sum_{i=1}^{N} Q_i(t) = \frac{1}{\Delta y}\sum_{i=1}^{N} S_i(\xi_i)u_{xi}\,. \tag{6.11}$$

This is a discrete version of (6.9), where we note that N, S_i and u_{xi} are random variables. Each of these quantities fluctuates with time. Also note that (6.11) is vertically integrated, so we are dividing by the length Δy rather than the area A, as is conventional in describing the flux over a surface.

We now distinguish two distributions of particle velocities. Let $f_{v_x}(v_x)$ denote the distribution of the velocities v_x of all particles in the vicinity of the surface A. This is to be considered an ensemble distribution with mean velocity $\langle v_x\rangle$ (e.g. Fathel et al., 2015). In turn let $f_{u_{xi}}(u_{xi})$ denote the distribution of all possible velocities u_{xi} of particles that intersect the surface A at any instant, as in (6.11). This distribution is to be considered a "sampling" distribution in the sense that it represents a set of particle velocities drawn from the distribution $f_{v_x}(v_x)$, coinciding with particles that intersect A. Under certain circumstances these two distributions are the same. But this is not generally the case.

Letting an overline denote an average over N particles, the last part of (6.11) may be written as $q_x = (1/\Delta y)N\overline{S_i(\xi_i)u_{xi}}$. For equal-sized particles, moreover, it is reasonable to assume that S_i and u_{xi} are uncorrelated, as there is no reason to suspect that, at any instant, particles intersecting A with large or small cross-sectional area S_i are any more or less likely to possess large or small velocity u_{xi}. In this case,

$$q_x(t) = \frac{1}{\Delta y}N\overline{S_i(\xi_i)}\,\overline{u_{xi}} = \frac{S}{\Delta y}\overline{u_{xi}} = \gamma\overline{u_{xi}} \tag{6.12}$$

The product $N\overline{S_i(\xi_i)} = S$ [L^2] is the cross-sectional area of the N particles intersecting A, and the ratio $S/\Delta y = \gamma$ [L^{-1}] is equivalent to the particle activity, the volume of active particles per unit streambed area. Specifically, this is a local "line" averaged activity. Because $S\mathrm{d}x$ is equal to the volume of active particles within a small spatial interval $\mathrm{d}x$, $S\mathrm{d}x/\mathrm{d}x\Delta y = S/\Delta y = \gamma$ is the volume of active particles within the small area $\mathrm{d}x\Delta y$. Then, if it is assumed that $\overline{u_{xi}}$ is equal to the average velocity $\langle v_x\rangle$ of all particles in the cloud in the vicinity of A, that is $\langle v_x\rangle = \overline{u_{xi}}$, one may conclude that

$$q_x = \gamma\langle v_x\rangle\,, \tag{6.13}$$

which is the definition of the flux normally assumed for quasi-steady bed and transport conditions (e.g. Bridge and Dominic, 1984; Wiberg and Smith, 1989; Seminara et al., 2002; Parker et al., 2003; Francalanci and Solari, 2007; Wong et al., 2007; Lajeunesse et al., 2010). However, several caveats must accompany this assessment of averages.

First, envision a uniform cloud of equal-sized particles moving with varying velocities parallel to x toward and through a set of surfaces A located at various positions along x. By "uniform" we mean the following. For a specified width Δy, let $n_x(x,t)$ [L^{-1}] denote the number of particles per unit distance parallel to x, such that $n_x(x,t)\mathrm{d}x$ is the number of particles whose noses are located within any small interval $\mathrm{d}x$. Then, for a sufficiently large width Δy, assume that $n_x(x,t)$ varies negligibly with x. At any instant the number of particles N and the corresponding particle area $S = N\overline{S_i}$ intersecting each surface is the same, although the detailed configuration of S varies from surface to surface. In this situation the sampling distribution $f_{u_{xi}}(u_{xi})$ is the same as the ensemble distribution $f_{v_x}(v_x)$ and the surface average $\overline{u_{xi}}$ is equal to the ensemble average $\langle v_x \rangle$. Because the cloud is uniform, each surface A samples at any instant the full distribution of possible velocities (for sufficiently large width Δy), in which case $\overline{u_{xi}} = \langle v_x \rangle$ for all surfaces.

In contrast, envision a cloud of particles with average velocity $\langle v_x \rangle$ whose concentration $n_x(x,t)$ at some instant decreases with increasing distance x. Now, both the number of particles N and the particle area $S = N\overline{S_i}$ intersecting each surface decrease with increasing x. Moreover, in this case the surface and ensemble averages of the velocity are not equivalent, with $\overline{u_{xi}} > \langle v_x \rangle$. Here is why.

Let a prime denote a deviation about an average. Then, at any instant $S_i = \overline{S_i} + S_i'$ and $u_{xi} = \langle v_x \rangle + u_{xi}'$. Notice that we are defining the deviation u_{xi}' with respect to the ensemble average $\langle v_x \rangle$ rather than the surface average $\overline{u_{xi}}$. In turn, $q_x = (1/\Delta y)N\left(\overline{S_i}\langle v_x \rangle + \overline{S_i}\,\overline{u_{xi}'} + \langle v_x \rangle \overline{S_i'} + \overline{S_i' u_{xi}'}\right)$. Consider a plot of u_{xi}' versus S_i' at an instant (Figure 6.4), which provides a perspective as viewed by an observer

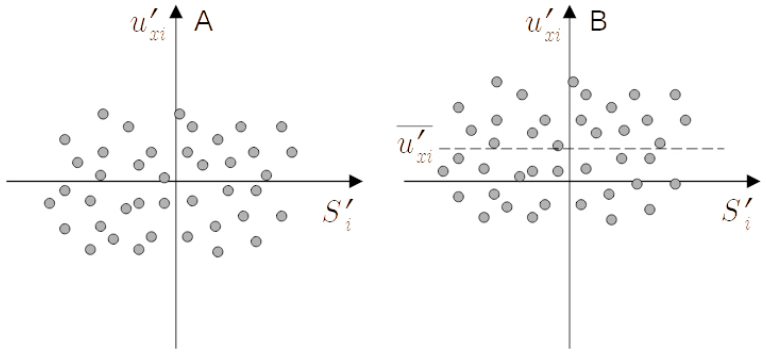

Figure 6.4: Plots of deviation in particle velocity $u_{xi}' = u_{xi} - \langle v_x \rangle$ versus deviation in particle cross-sectional area $S' = S_i - \overline{S_i}$ as viewed by observer moving with the average velocity $\langle v_x \rangle$ for (A) uniform particle cloud with $\overline{u_{xi}'} = 0$ and $\overline{u_{xi}} = \langle v_x \rangle$, and (B) particle cloud where the particle activity decreases with increasing distance x with $\overline{u_{xi}'} > 0$ and $\overline{u_{xi}} > \langle v_x \rangle$.

moving with the average velocity $\langle v_x \rangle$, although the conclusions presented next pertain equally to an Eulerian frame of reference. During a small interval of time $\mathrm{d}t$, some points on this plot move to the right as the cross-sectional area S_i' increases for particles that are beginning to cross A, and some points move to the left as the cross-sectional area S_i' decreases for particles that have mostly crossed A. The rate of motion of the points to the right and left is proportional to the magnitude of the particle velocity u_{xi}', so motion is faster near the top and bottom and slower near the middle of the plot. Points at $u_{xi}' = 0$ along the S_i' axis do not move during $\mathrm{d}t$. Some points vanish as particles leave A, and new points appear as particles arrive at and initially intersect A. Points arrive at the far left of the second and third quadrants where the small areas of intersection of arriving particles are less

than the average intersection area, and move to the far right of the first and fourth quadrants as their fat middles exceed the average intersection area, and then move back to the far left of the second and third quadrants because the intersection area of their exiting tails is less than the average intersection area.

In the case of the uniform cloud of particles described above, the number of points and their scatter is similar across all surfaces A and on each surface over time. Thus, $\overline{u_{xi}} = \langle v_x \rangle$ with $\overline{S_i}\,\overline{u'_{xi}} = \langle v_x \rangle \overline{S'_i} = \overline{S'_i u'_{xi}} = 0$ (Figure 6.4), so that $q_x = (1/\Delta y) N \overline{S_i(\xi_i)}\,\overline{u_{xi}} = \gamma\,\overline{u_{xi}} = \gamma \langle v_x \rangle$ as in (6.12) or (6.13). In the second case where the particle activity decreases with increasing x, this situation changes. At any instant the number of particles to the immediate left of A is greater than the number to the immediate right of A. The likelihood that a particle to the left or right of A will intersect A during a small interval of time $\mathrm{d}t$, for a given magnitude of the velocity u'_{xi}, increases with its proximity to A, and, for a given proximity to A, increases with the magnitude of its velocity u'_{xi}. Of the particles that are at any given distance to the left of A, the faster ones (large positive u'_{xi}) are more likely than are slower ones to reach A. And, of the particles that are at any given distance to the right of A, the slower ones (large negative u'_{xi}) are more likely than are faster ones to reach A. Because of the greater number of particles to the left of A than to the right of A, the plot of u'_{xi} versus S'_i becomes preferentially populated by faster moving particles and depleted of slower moving particles. The effect is to shift the surface-averaged velocity $\overline{u_{xi}}$ upward such that $\overline{u'_{xi}}$ is finite (Figure 6.4). That is, the surface A "sees" an average velocity $\overline{u_{xi}} > \langle v_x \rangle$ where $\overline{u_{xi}} = \langle v_x \rangle + \overline{u'_{xi}}$ with $\langle v_x \rangle \overline{S'_i} = \overline{S'_i u'_{xi}} = 0$ for the same particle surface area $S = N\overline{S_i}$. In turn, the flux

$$q_x = \frac{1}{\Delta y} N \left(\overline{S_i} \langle v_x \rangle + \overline{S_i}\,\overline{u'_{xi}} \right) = \gamma \langle v_x \rangle + \gamma \overline{u'_{xi}}\,, \tag{6.14}$$

in which an extra term involving velocity fluctuations about the mean appears in the definition of q_x. Note that this is equivalent to $q_x = \gamma \overline{u_{xi}}$, as it must be according to the definition (6.12). The counterpart to this situation occurs when the particle activity γ increases with distance x, in which case $\overline{u_{xi}} < \langle v_x \rangle$.

Here is an Eulerian interpretation. We again envision a situation in which the number density $n_x(x)$ varies with x, but now is steady. For a fixed area A the particle area $S = N\overline{S_i}$. If $n_x(x)$ is uniform, then for a sufficiently large width Δy the surface A samples all possible velocities with mean $\langle v_x \rangle$ such that the distributions $f_{u_{xi}}(u_{xi})$ and $f_{v_x}(v_x)$ are the same and $\overline{u_{xi}} = \langle v_x \rangle$ with $\overline{u'_{xi}} = 0$. At any time t the particles intersecting A started their motions at time $t - \mathrm{d}t$ from varying positions x_i upstream from A. These distances are $x_i = u_{xi}\mathrm{d}t = (\langle v_x \rangle + u'_{xi})\mathrm{d}t$. Thus, x_i is large with large u_{xi} and $u'_{xi} > 0$, and x_i is small with small u_{xi} and $u'_{xi} < 0$. In this case $q_x = \gamma \langle v_x \rangle$.

In contrast, if $n_x(x)$ decreases with increasing x, then the average velocity of particles intersecting A is $\overline{u_{xi}} > \langle v_x \rangle$. At any time t particles intersecting A started their motions from varying distances x_i upstream. But now, because there are more active particles upstream from A than at A, the number of particles reaching A at time t which started "far" upstream increases. That is, a greater proportion of the N particles intersecting A at time t involves faster particles than with uniform $n_x(x)$, and a smaller proportion involves slower particles. Relative to the ensemble distribution $f_{v_x}(v_x)$, the distribution $f_{u_{xi}}(u_{xi})$ of velocities u_{xi} intersecting A is skewed to faster particles. As a consequence, $\overline{u_{xi}} > \langle v_x \rangle$ and $\overline{u'_{xi}} > 0$. Note that this effect is not because of a change in the ensemble distribution of velocities with mean $\langle v_x \rangle$. Rather, it is a consequence of the variation in the number density $n_x(x)$ and thus the particle activity γ. The distribution $f_{u_{xi}}(u_{xi})$ of velocities u_{xi} presented to A is different than the distribution $f_{v_x}(v_x)$ of velocities of all particles in the vicinity of A.

This effect of an activity gradient vanishes in the absence of fluctuating particle velocities (i.e. if $\overline{u'_{xi}} = 0$), and, as elaborated in Chapter 7, this effect represents diffusion when particle motions are cast in probabilistic terms. We in fact show that whereas $(1/\Delta y) N \overline{S_i} \langle v_x \rangle = \gamma \langle v_x \rangle$ represents advection, the product $(1/\Delta y) N \overline{S_i}\,\overline{u'_{xi}} = \gamma \overline{u'_{xi}}$ represents a diffusive term that looks like $-\partial(\kappa\gamma)/\partial x$, where κ [L^2

T^{-1}] is an Eulerian particle diffusivity.

A second caveat concerns the particle activity. In the development above we imagined large Δy, and therefore large N, in order to compare the sampling distribution $f_{u_{xi}}(u_{xi})$ with the ensemble distribution $f_{v_x}(v_x)$. But recall that with finite length Δy, N and S_i, and therefore S and γ, are random variables. As described in Chapter 7, this means that we must envision the flux as an ensemble average and write it as

$$\langle q_x \rangle = \langle \gamma \rangle \langle v_x \rangle - \frac{\partial}{\partial x} \left(\kappa \langle \gamma \rangle \right) , \tag{6.15}$$

where now the activity is averaged. In turn, we must envision the flux given by (6.15) as representing an *expected* value. As such $\langle q_x \rangle$ does *not* describe what occurs within any individual realization. We examine the implications of this at several points in the book. Moreover, we show in Chapter 7 that the definition of the flux (6.15) also emerges from a master equation that describes the time evolution of the probability distribution of active particle positions.

A third caveat that goes with the averaging above centers on particle size. As mentioned above, for equal-sized particles it may be assumed that S_i and u_{xi} are uncorrelated. When considering a mixture of particle sizes, however, the covariance between S_i and u_{xi} cannot be neglected inasmuch as some particle sizes preferentially move faster than other sizes. As elaborated in Chapter 12, this means that individual sizes must be treated separately.

For a given particle volume V_p the particle number flux q_{nx} [L^{-1} T^{-1}] is obtained by dividing (6.15) by V_p. This gives

$$\langle q_{nx} \rangle = \langle \gamma_n \rangle \langle v_x \rangle - \frac{\partial}{\partial x} \left(\kappa \langle \gamma_n \rangle \right) , \tag{6.16}$$

where $\langle \gamma_n \rangle$ [L^{-2}] is the averaged particle number activity. In turn, (6.16) represents the expected value for individual realizations of the averaged time series I given by (6.4), conditioned on the length Δy and the averaging interval Δt.

As noted above the activity form of the particle flux, as a product of the locally averaged particle activity and velocity, is continuum-like in its conceptualization. Nonetheless, the form given by (6.16) embodies a fundamentally different behavior. In a continuum fluid, frequent particle–particle collisions maintain uniform particle number densities at the continuum scale (Chapter 1). Fluctuations in number density at a smaller scale are short-lived. This means that particle diffusion in a fluid is not relevant and the continuum flux is entirely advective when viewed at the Knudsen scale or larger. This mechanism of homogenization by particle–particle collisions does not occur in rarefied sediment systems, wherein effects embodied in the diffusive term in (6.16) must be taken into account.

6.3.2 Entrainment Form

In contrast to the activity form of the particle flux, the entrainment form is centered on the kinematics of particle motions in relation to entrainment and disentrainment.[4] This form therefore highlights the elements of the phase transitions of transport as described in Chapter 1, and it embodies the idea of "nonlocal" transport, to mean that the flux at a position x at time t may be viewed as the outcome of conditions that influence the entrainment of particles from upstream or upslope positions $x' < x$, as well as their travel to and arrival at x at time t (Section 6.5). In the following we assume ensemble behavior, to mean that the probability distributions describing characteristic features of particle motions (e.g. particle velocities, hop distances, and travel times) are a signature of the transport process for given sediment properties and external controlling factors. For simplicity we focus on particle motions in one direction.

Let $f_{L_x,T_\mathrm{p}}(L_x, T_\mathrm{p}; x', t')$ denote the joint ensemble distribution of particle hop distances L_x and associated travel times T_p for particles whose motions start at position x' at time t'. These quantities

[4] Much of the material in this section comes from Furbish et al. (2017a).

generally are correlated (Roseberry et al., 2012; Fathel et al., 2015; Wu et al., 2020). We now define a conditional probability density as

$$f_{L_x|T_\mathrm{p}}(L_x|T_\mathrm{p};x',t') = \frac{f_{L_x,T_\mathrm{p}}(L_x,T_\mathrm{p};x',t')}{f_{T_\mathrm{p}}(T_\mathrm{p};x',t')}\,, \tag{6.17}$$

where $f_{T_\mathrm{p}}(T_\mathrm{p};x',t')$ is the marginal distribution of $f_{L_x,T_\mathrm{p}}(L_x,T_\mathrm{p};x',t')$ representing the travel times T_p. In turn we define a conditional survival function as $R_{L_x|T_\mathrm{p}}(L_x|T_\mathrm{p};x',t') = 1 - F_{L_x|T_\mathrm{p}}(L_xT_\mathrm{p};x',t')$, where

$$F_{L_x|T_\mathrm{p}}(L_x|T_\mathrm{p};x',t') = \int_0^{L_x} f_{L_x|T_\mathrm{p}}(L_x'|T_\mathrm{p};x',t')\,\mathrm{d}L_x' \tag{6.18}$$

is a conditional cumulative distribution function, and the prime on L_x denotes this as the variable of integration. We now observe that, so long as $f_{L_x|T_\mathrm{p}}(L_x|T_\mathrm{p};x',t')$ possesses finite first and second moments (i.e. it is not heavy tailed), the conditionally expected hop distance, $L_{x1}(T_\mathrm{p};x',t' = \mathrm{E}(L_x|T_\mathrm{p};x',t')$, is given by (Furbish and Haff, 2010; Furbish and Roering 2013)

$$L_{x1}(T_\mathrm{p};x',t' = \mathrm{E}(L_x|T_\mathrm{p};x',t') = \int_0^\infty R_{L_x|T_\mathrm{p}}(L_x|T_\mathrm{p};x',t')\,\mathrm{d}L_x\,, \tag{6.19}$$

and the conditionally expected second moment, $L_{x2}(T_\mathrm{p};x',t') = \mathrm{E}(L_x^2|T_\mathrm{p};x',t')$, is given by

$$L_{x2}(T_\mathrm{p};x',t') = \mathrm{E}(L_x^2|T_\mathrm{p};x',t') = 2\int_0^\infty L_xR_{L_x|T_\mathrm{p}}(L_x|T_\mathrm{p};x',t')\,\mathrm{d}L_x\,. \tag{6.20}$$

These definitions become useful below.

Let $E_n(x',t')$ denote a Poisson-like rate of particle entrainment per unit sediment-surface area at the position x' at time t'. This is an expected value that is either constant or changes vary slowly with time, thus maintaining quasi-steady conditions. Then, during a small interval $\mathrm{d}t'$ the expected number of particles entrained from the sediment-surface area $\Delta y\mathrm{d}x'$ is $\Delta y\mathrm{d}x'\mathrm{d}t'E(x',t')$. Of these entrained particles, the number of particles that possess a travel time within the interval T_p to $T_\mathrm{p} + \mathrm{d}T_\mathrm{p}$ is $\Delta y\mathrm{d}x'\mathrm{d}t'E_n(x',t')f_{T_\mathrm{p}}(T_\mathrm{p};x',t')\mathrm{d}T_\mathrm{p}$, and the expected number of particles possessing this travel time which also move at least as far as L_x is

$$\Delta y\mathrm{d}x'\mathrm{d}t'E_n(x',t')f_{T_\mathrm{p}}(T_\mathrm{p};x',t')\mathrm{d}T_\mathrm{p}R_{L_x|T_\mathrm{p}}(L_x|T_\mathrm{p};x',t')\,. \tag{6.21}$$

The particles described by (6.21) by definition must move past the position $x = x' + L_x$ at times t such that $t' \le t \le t' + T_\mathrm{p}$. That is, crossings of x generally do not occur at the same time. Nonetheless, with steady entrainment and transport conditions, conservation of mass requires that particles entrained within $\Delta y\mathrm{d}x'$ according to (6.21) must contribute a steady stream of particles moving past the position $x = x' + L_x$ during a specified interval of time $\mathrm{d}t$. Because the expected number is fixed for any specified interval of time we may set $\mathrm{d}T_\mathrm{p} = \mathrm{d}t$ and consider all possible displacements L_x and associated travel times T_p of particles entrained at all possible starting positions x' and times t'. The expected number of particles crossing the position x during a small interval $\mathrm{d}t$ is then

$$\mathrm{d}N = \Delta y\mathrm{d}t\int_{-\infty}^{t}\int_{-\infty}^{x} E_n(x',t')f_{T_\mathrm{p}}(T_\mathrm{p};x',t')R_{L_x|T_\mathrm{p}}(L_x|T_\mathrm{p};x',t')\,\mathrm{d}x'\,\mathrm{d}t'\,, \tag{6.22}$$

in which $T_\mathrm{p} = t - t'$ and $L_x = x - x'$. That is, (6.22) accumulates the small number of particles $\mathrm{d}N$ entrained from all possible positions x' at previous times t' which move at least as far as x by time t during any interval $\mathrm{d}t$. Then, because the expected particle number flux $\langle q_{nx}(x,t)\rangle = (1/\Delta y)\mathrm{d}N/\mathrm{d}t$,

$$\langle q_{nx}(x,t)\rangle = \int_{-\infty}^{t}\int_{-\infty}^{x} E_n(x',t')f_{T_\mathrm{p}}(T_\mathrm{p};x',t')R_{L_x|T_\mathrm{p}}(L_x|T_\mathrm{p};x',t')\,\mathrm{d}x'\,\mathrm{d}t'\,. \tag{6.23}$$

This is an expression of the entrainment form of the expected particle flux. It requires knowledge of the entrainment rate, the distribution of particle travel times and the distribution of hop distances conditioned on travel times, each of which may vary with position assuming quasi-steady conditions.

Note that (6.23) is a nonlocal expression of the expected flux (see Section 6.5). It explicitly acknowledges that particles contributing to the flux at x at time t started their motions at upstream or upslope positions $x' = x - L_x$ at previous times $t' = t - T_\mathrm{p}$. Further note that this expression is scale independent.

Although (6.23) is a precise probabilistic description of the expected flux, it is not necessarily useful in this form. Let us therefore consider an approximation of (6.23) having the form of an advection–diffusion equation, which provides a valuable perspective on the idea of nonlocal transport (Section 6.5). With $x' = x - L_x$ and $t' = t - T_\mathrm{p}$, and noting that $\mathrm{d}x' = \mathrm{d}x = \mathrm{d}L_x$ and $\mathrm{d}t' = \mathrm{d}T_\mathrm{p}$, then a change of variables in (6.23) leads to

$$\langle q_{nx}(x,t)\rangle =$$

$$\int_0^\infty \int_0^\infty E_n(x - L_x, t - T_\mathrm{p}) f_{T_\mathrm{p}}(T_\mathrm{p}; x - L_x, t - T_\mathrm{p}) R_{L_x|T_\mathrm{p}}(L_x|T_\mathrm{p}; x - L_x, t - T_\mathrm{p})\, \mathrm{d}L_x\, \mathrm{d}T_\mathrm{p}\,. \tag{6.24}$$

Assuming that E_n, $f_{T_\mathrm{p}}(T_\mathrm{p})$ and $R_{L_x|T_\mathrm{p}}(L_x|T_\mathrm{p})$ change negligibly (or in a quasi-steady manner) with time, we may neglect the time dependence in (6.24). We then expand the integrand as a Taylor series to first order only with respect to x, and, with appropriate factoring obtain

$$\begin{aligned} \langle q_{nx}(x)\rangle &= E_n(x) \int_0^\infty f_{T_\mathrm{p}}(T_\mathrm{p}; x) \int_0^\infty R_{L_x|T_\mathrm{p}}(L_x|T_\mathrm{p}; x)\, \mathrm{d}L_x\, \mathrm{d}T_\mathrm{p} \\ &- \frac{\partial}{\partial x}\left[E_n(x) \int_0^\infty f_{T_\mathrm{p}}(T_\mathrm{p}; x) \int_0^\infty L_x R_{L_x|T_\mathrm{p}}(L_x|T_\mathrm{p}; x)\, \mathrm{d}L_x\, \mathrm{d}T_\mathrm{p} \right]. \end{aligned} \tag{6.25}$$

Using the definitions of expectations given by (6.19) and (6.20) together with the law of the unconscious statistician (Chapter 2) then leads to

$$\langle q_{nx}(x)\rangle = E_n \langle L_x\rangle - \frac{1}{2}\frac{\partial}{\partial x}\left(E_n \langle L_x^2\rangle \right), \tag{6.26}$$

which is an advection–diffusion approximation of (6.23). Here it is important to recognize that $\langle L_x^2\rangle$ is the raw variance of the hop distances, that is, the second moment measured about the origin, rather than the ordinary variance measured about the average.

The diffusive term in (6.26) is an approximation of the nonlocal behavior embodied in (6.23). In effect this term "looks" at conditions upstream of x, and takes into account the effect of variations in these conditions relative to those at x. This term is not diffusive in the classic sense of molecular diffusion. Although it describes effects of spatial variations in the excitation of particles (via E_n) and deviations in particle displacements about the average (via $\langle L_x^2\rangle$), analogous to molecular diffusion, it is more accurate to think of this term as modulating the advective term in (6.26). Moreover, it is possible to show (Chapter 8) that this approximation is very good so long as $\langle L_x\rangle \ll \lambda_1$, where the characteristic length λ_1 is defined as

$$\lambda_1 = \frac{\left| \mathrm{d}\left(E_n \langle L_x^2\rangle \right) / \mathrm{d}x \right|}{\left| \mathrm{d}^2\left(E_n \langle L_x^2\rangle \right) / \mathrm{d}x^2 \right|}, \tag{6.27}$$

which is a measure of the distance over which the gradient $\mathrm{d}\left(E_n \langle L_x^2\rangle \right) / \mathrm{d}x$ changes. Inasmuch as the numerator in (6.27) is constant over a distance $\lambda_1 \gg \langle L_x\rangle$, then in the limit of $\lambda_1 \to \infty$, (6.26) converges to the flux described by (6.23).

For nominally uniform, steady conditions (6.26) yields the definition of the flux introduced by Einstein (1950). Namely,

$$\langle q_{nx}\rangle = E_n \langle L_x\rangle, \tag{6.28}$$

although Einstein did not formally treat this as the expected value of a stochastic process involving an ensemble of possible realizations, as described in Chapter 4.

It is important to reemphasize that the Poisson-like entrainment rate E_n is an expected value and that the joint distribution of displacements L_x and associated travel times T_p is an ensemble distribution. We are therefore envisioning the expected flux given by (6.26) as an abstraction such that E_n and the moments $\langle L_x \rangle$ and $\langle L_x^2 \rangle$ are, as ensemble averaged quantities, continuously differentiable with respect to space.[5] As such, $\langle q_{nx} \rangle$ does *not* describe what occurs within any individual realization. Also recall from Section 6.2 that the probabilistic properties of such realizations hinge on the resolution of measurements — the lengths Δx and Δy, and the averaging interval Δt. We examine the implications of this at several points in the book. Moreover, we show in Chapter 7 that the definition of the flux (6.26) also emerges from a master equation used to obtain the entrainment form of the Exner equation.

6.3.3 Key Contrasts and Applications

The two definitions of the particle flux presented above represent fundamentally different kinematic views of the transport process. Here we highlight key contrasts in these definitions, and then return to them when we obtain definitions of the particle flux that emerge from master equations centered on probabilistic descriptions of particle positions and motions (Chapter 7).

The particle flux is of course a rate, which is emphasized when we refer to it as a particle number or a particle volume per unit length *per unit time*. This attribute is embedded differently in the two definitions of the flux. In the activity form the rate attribute is contained in the particle velocity $\langle v_x \rangle$ [L T^{-1}]. In the entrainment form the rate attribute is contained in the entrainment rate E_n [L^{-2} T^{-1}]. The activity definition thus views the speed of the process, the flux, as being set by the particle velocity in concert with the number of active particles. The entrainment definition instead views the speed of the process as being set by the rate of particle excitation, that is, the rate at which particles are set in motion in concert with their displacements.

In the definition of the activity form of the particle flux given by (6.15) or (6.16), the product of the particle activity and the average particle velocity is continuum-like in concept. This product is a purely kinematic expression of what is occurring, on average, at a control surface A. Each of the particles reaching the surface A and contributing to these averages possesses a unique history consisting of its starting position with entrainment, its velocity fluctuations in response to particle–surface collisions or turbulence, or both, and its travel distance and associated travel time. Yet the averages in (6.15) or (6.16) reflect nothing about these individual histories that occur upstream or upslope from the surface A, nor anything about the collective (averaged) history of the particles. The diffusive term, via the derivative, indeed "looks" upstream or upslope to register spatial variations in active particle numbers. But this is the only information regarding conditions "far" from the surface A that influence the flux at A. As a consequence, the activity form of the flux is effectively removed from the physics of the phase transitions — entrainment and disentrainment — that fundamentally regulate rarefied particle transport (Chapter 1). The particle activity must be described separately in relation to particle entrainment and deposition (Chapters 7 and 12), and similarly the average particle velocity must be obtained separately from considerations of the statistical mechanics of particle velocity states (Chapter 12). The activity definition is then just the algebraic relation required to give the expected flux.

In contrast, the processes of entraiment and disentrainment are central to the definition (6.23) of the entrainment form of the particle flux and its advection–diffusion approximation (6.26). This definition explicitly "looks" at upstream or upslope conditions, including starting positions, and provides the kinematic basis for describing particle disentrainment as manifest in the distribution of particle displacements L_x and thus the exceedance probability function $R_{L_x|T_\mathrm{p}}(L_x|T_\mathrm{p})$. However, by focusing

[5] This does *not* imply continuum-like conditions. Indeed, the entrainment rate E_n is resolved at lengths Δx and Δy and is undefined in the limit of $\Delta x, \Delta y \to 0$.

on the phase transitions, this definition says little about the particle activity; and in focusing on integrated quantities (displacements), it says little about the details of particle motions in reaching a surface A. This information is embedded in separate descriptions of the statistical mechanics of disentrainment leading to the distribution of particle displacements, as previously outlined in our description of survival analysis (Chapter 4).

With rarefied particle motions on hillslopes (Chapter 10), particle excitation generally is patchy and highly intermittent. Particle travel times are negligible relative to the reciprocal of the excitation recurrence frequency. The idea of an average particle activity associated with coordinate position therefore is not meaningful, and particle velocities only figure into the mechanics of disentrainment. Likewise, with rain splash transport, particle displacements following raindrop impacts occur within one-tenth of a second, an interval that is negligible relative to the reciprocal of the impact frequency within an area comparable to the square of the average particle displacement (Chapter 11). Moreover, despite our intuition that raindrops during a heavy storm quickly fill a specified area of the land surface, in fact impact locations are highly patchy relative to the scale of most particle motions. Again, the idea of an average particle activity associated with coordinate position is an abstraction, and particle velocities only figure into descriptions of particle displacements.[6] For these reasons the entrainment form of the particle flux is the unambiguous choice, as this definition explicitly addresses the essential elements involved: the excitation and travel distances of the particles, taking into account upslope and downslope conditions that influence these distances. Clarifying the mechanics and rates of particle excitation constitutes the foremost challenge in describing these processes.

With soil particles, including tracer particles, conditions are continuum-like with respect to particle numbers, but only in the sense of an ensemble averaged configuration and behavior (Chapter 14), not as we might envision with an individual realization of a granular fluid. The entrainment form of the flux, focused on particle exchanges at a sediment–fluid interface, is not meaningful. Here a suitable form of the activity definition of the flux is the appropriate choice, although this requires taking into account the highly intermittent excitation of particles by disturbances in concert with athermal granular creep. The particle activity defined above in relation to a sediment–fluid interface is replaced with a volumetric version, and the averaged velocity is redefined as a virtual particle velocity. Because of the relatively slow pace of collective soil particle motions combined with the patchiness and intermittency of disturbances, ensemble averaging becomes essential in the interpretation of the particle flux and the behavior of tracer particles.

With bed load transport, the two definitions of the particle flux in fact point to certain elements of particle motions that require clarification for understanding transport. The entrainment definition is in many respects ideally suited to rarefied transport conditions. It provides the basis for treating the flux as a counting process, querying upstream conditions that influence particle motions. A current weakness resides in specifying the stochastic structure of the entrainment rate in relation to flow conditions and bed-surface structure; and particle excitation may in part depend on the particle activity inasmuch as moving particles are involved in collective entrainment. In addition, much still needs to be learned about the mechanics of particle disentrainment in setting the distributions of particle displacements. Likewise the particle activity depends on entrainment in competition with deposition, and particle velocities are not just related to near-bed flow conditions. Particle velocities are strongly influenced by particle–surface interactions in concert with flow and thus share the mechanics of disentrainment (Chapter 12). As with transport on hillslopes, clarifying the mechanics and rates of particle excitation constitutes a primary challenge in describing bed load transport, notably in considering transport at time scales much larger than experimental time scales.

[6] Whereas rain splash transport can be formally described in terms of the activity form of the particle flux (Furbish et al., 2009a), the kinematic elements of the entrainment form provide a more tangible physical interpretation of the flux.

6.4 Properties of Time Averaging

6.4.1 Uncertainty with Time Averaging

An oft reported observation is that measurements of bed load transport obtained at relatively high temporal resolution characteristically exhibit large fluctuations over a broad range of frequencies (e.g. Gomez and Church, 1989; Hassan and Church, 2000; Singh et al., 2009; Dhont and Ancey, 2018; Chartrand, 2017; Ancey and Pascal, 2020; Hassan et al., 2022; Fan et al., 2023; Li et al., 2023). Various factors contribute to these fluctuations in transport. Importantly, as should now be clear from material presented in previous chapters, such fluctuations must be viewed as an *inherent feature* of transport owing in part to the small numbers of particles involved in rarefied conditions. This variability does not merely represent effects of unexplained stochastic influences — "noise" — about deterministically conceptualized descriptions of the transport rate.

On this matter, measurements of time series of sediment transport involve a compelling problem: how the measurement interval Δt influences our understanding and interpretation of the particle flux. This notably includes how averaging over Δt influences the rate of convergence of estimates of the flux to the expected value (Ancey and Pascal, 2020; Furbish and Doane, 2021; Figures 1.1, 1.2 and 6.2), and the related observation that the variance of the flux systematically varies with the sampling interval Δt (Singh et al., 2009; Ma et al., 2014). For bed load transport in particular, Ma et al. (2014) suggest that the variance of the flux scales differently over three characteristic time scales: a short "intermittent stage" in which crossing events appear Poissonian; an "invariant stage" in which effects of burstiness increase the strength of the fluctuations in the flux; and a "memoryless stage" in which the variance of the averaged flux again grows linearly with increasing sampling time in a Poissonian manner. Based on the stochastic birth-death formulation of transport developed by Ancey et al. (2008; see Chapter 12) they describe the flux as a Cox process (or doubly stochastic Poisson process), which is basically an inhomogeneous Poisson process in which the Poisson rate $\lambda(t)$ is itself a stochastic process. A key ingredient leading to this scaling behavior in their analysis is collective entrainment (Ancey et al., 2008; Ancey and Heyman, 2014; Lee and Jerolmack, 2018) related to hydrodynamic interactions between moving particles and the bed, particle–bed collisions, and possibly cascading effects of adjustments in surface texture and configuration (e.g. Singh et al., 2009; Masteller and Finnegan, 2017; Yager et al., 2018) including migration of bedforms or bedform-like features.

In later chapters we examine several counting processes in describing the particle flux and its divergence, and associated uncertainties, including the behavior described by Ma et al. (2014). Here we start by illustrating how the expected value and the variance of realizations of the number $N(\Delta t)$ and the particle flux $q_{nx}(\Delta t)$ vary with the measurement interval Δt. We compare properties of homogeneous Poisson and compound Poisson processes, and a simple homogeneous renewal process. We then turn to simple inhomogeneous processes and show that the essence of the behavior described by Ma et al. (2014), as summarized above, generally occurs with a time-varying Poisson intensity $\lambda(t)$, whether as a deterministic function or as a stochastic process. Our objective is to highlight shared properties of these processes in aiming at interpretations of time series of particle transport, with clear implications for sampling.

Homogeneous Conditions

This brief section on homogeneous conditions is in part a review of material covered in Chapter 4, as context for what follows. A homogeneous Poisson process serves as the starting point. The distribution $f_w(w)$ of independent wait times w (or inter-arrival or inter-event times) between successive events is exponential with mean μ_w and variance $\sigma_w^2 = \mu_w^2$. The Poisson intensity $\lambda = 1/\mu_w$. For a fixed Poisson intensity λ and interval Δt the number of events $N(\Delta t)$ is described by a Poisson distribution with expected value $\mathrm{E}[N(\Delta t)] = \lambda \Delta t$ and variance $\mathrm{Var}[N(\Delta t)] = \lambda \Delta t$ (Figure 6.5). In turn, the variance

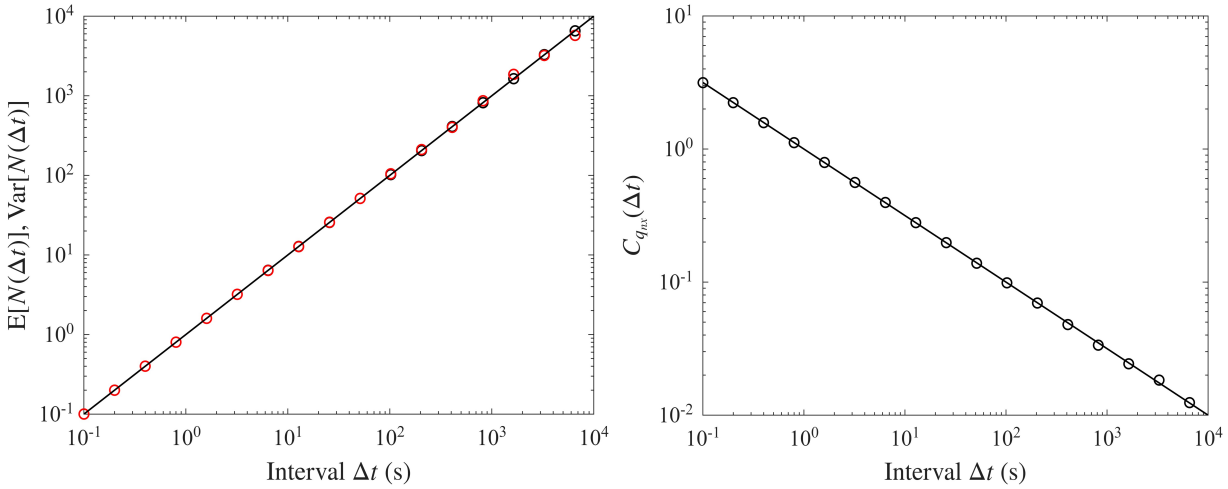

Figure 6.5: Plot of (left) expected value $\mathrm{E}[N(\Delta t)]$ and variance $\mathrm{Var}[N(\Delta t)]$ of the number $N(\Delta t)$ versus time interval Δt for a homogeneous Poisson process with intensity $\lambda = 1$ s^{-1} together with synthetically generated expected values (black circles) and variances (red circles); and plot of (right) coefficient of variation $C_{q_{nx}}$ of the flux q_{nx} versus time interval Δt together with synthetically generated values (circles).

of the flux $\mathrm{Var}[q_{nx}(\Delta t)] = \lambda/\Delta t$ and the coefficient of variation is (Figure 6.5)

$$C_{q_{nx}} = \frac{1}{\sqrt{\lambda \Delta t}} \,. \tag{6.29}$$

Note the large uncertainty at small Δt as measured by $C_{q_{nx}}$, in this example decreasing to 0.1 only by $\Delta t = 100$ s and to 0.01 only by $\Delta t = 10\,000$ s, or 2.8 hr. Values of $C_{q_{nx}}$ are displaced upward with decreasing intensity λ and downward with increasing λ. The synthetic values in this figure are calculated for non-overlapping intervals Δt in a long series of total length T. Because the number of intervals n decreases with increasing Δt as $n = T/\Delta t$, some variability from predicted values is apparent at large Δt.

These results provide a baseline for other processes. Also note that we focus here on the coefficient of variation (rather than just the variance) because this coefficient converges to zero at the same rate as the so-called standard error of the estimate of the mean.

Consider a homogeneous compound Poisson process with event rate λ_c. Let $p_{n_\mathrm{c}}(n_\mathrm{c})$ denote the compounding distribution of the number of particles $n_\mathrm{c} = 1, 2, 3, ...$ associated with each Poisson event. This number is independent of the Poisson events. It has the expected value $\langle n_\mathrm{c} \rangle$ and variance $\sigma^2_{n_\mathrm{c}}$. If $N_\mathrm{c}(t)$ is the number of Poisson events at time t with $N_\mathrm{c}(0) = 0$, then the total number $N(t)$ of crossing events of a compound Poisson process is defined as

$$N(t) = \sum_{i=1}^{N_\mathrm{c}(t)} n_{\mathrm{c}i} \,. \tag{6.30}$$

For a measurement interval Δt the expected number $\mathrm{E}[N(\Delta t)] = \langle n_\mathrm{c} \rangle \lambda_\mathrm{c} \Delta t$ and the variance $\mathrm{Var}[N(\Delta t)] = \langle n_\mathrm{c}^2 \rangle \lambda_\mathrm{c} \Delta t$ with raw variance $\langle n_\mathrm{c}^2 \rangle = \langle n_\mathrm{c} \rangle^2 + \sigma^2_{n_\mathrm{d}}$ (Figure 6.6). In turn the variance of the particle flux $\mathrm{Var}[q_{nx}(\Delta t)] = \langle n_\mathrm{c}^2 \rangle \lambda_\mathrm{c} / \Delta t$ and the coefficient of variation is (Figure 6.6)

$$C_{q_{nx}} = \sqrt{1 + \frac{\sigma^2_{n_\mathrm{c}}}{\langle n_\mathrm{c} \rangle^2}} \frac{1}{\sqrt{\lambda_\mathrm{c} \Delta t}} \,. \tag{6.31}$$

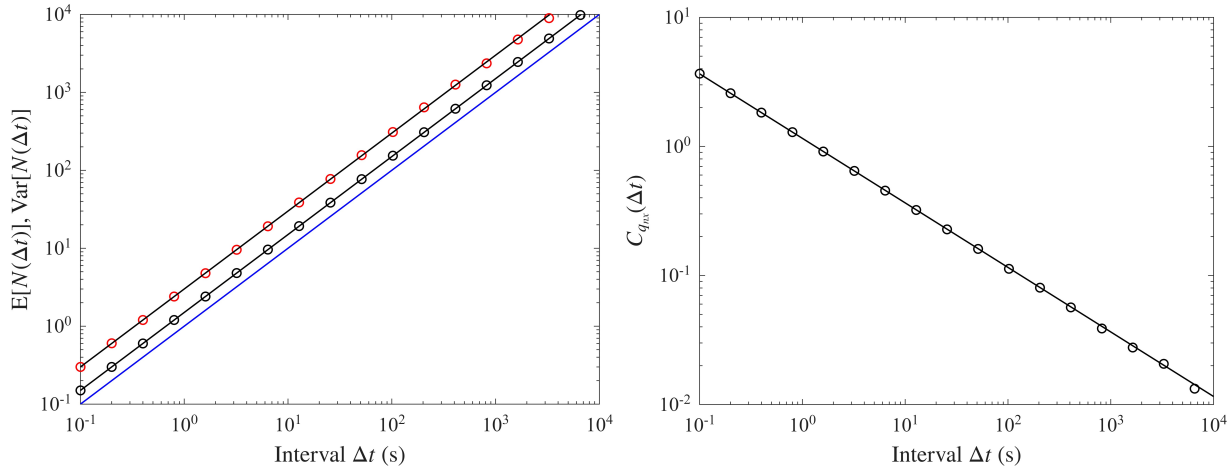

Figure 6.6: Plot of (left, black lines) expected value $\mathrm{E}[N(\Delta t)]$ and variance $\mathrm{Var}[N(\Delta t)]$ of the number $N(\Delta t)$ versus time interval Δt for a homogeneous compound Poisson process with (blue line) Poisson intensity $\lambda_\mathrm{c} = 1\ \mathrm{s}^{-1}$ together with synthetically generated expected values (black circles) and variances (red circles), where the compounding distribution is geometric with mean $\langle n_\mathrm{c}\rangle = 1.5$; and plot of (right) coefficient of variation $C_{q_{nx}}$ of the flux q_{nx} versus time interval Δt together with synthetically generated values (circles).

Because $\sqrt{1 + \sigma_{n_\mathrm{c}}^2/\langle n_\mathrm{c}\rangle^2} \geq 1$ the coefficient of variation generally converges to zero more slowly than in the case of a Poisson process (Figure 6.5). When $p_{n_\mathrm{c}}(n_\mathrm{c}) = 1$ for any $n_\mathrm{c} \geq 1$ with $\sigma_{n_\mathrm{c}}^2 = 0$ then (6.31) reduces to (6.29).

Consider a simple renewal process, and recall from Chapter 4 that this is a counting process in which the distribution $f_w(w)$ of wait times w has any form with positive support that is not exponential, so long as its mean μ_w is finite. A Poisson processes thus may be considered a special case of a renewal process, and a renewal process may be compounded (e.g. Ancey and Pascal, 2020). Also recall that the expected rate converges to $\lambda_\mathrm{r} = 1/\mu_w$ at large times, analogous to a homogeneous Poisson process (e.g. Nakagawa, 2011). The expected number $\mathrm{E}[N(\Delta t)] = \lambda_\mathrm{r}\Delta t$ and the variance $\mathrm{Var}[N(\Delta t)] = (\sigma_w^2/\mu_w^3)\Delta t = (\sigma_w^2/\mu_w^2)\lambda_\mathrm{r}\Delta t$ (Figure 6.7). In this example of a Weibull process, events are sufficiently sparse that the smallest intervals Δt mostly contain no events or only one event, and the distribution of events is indistinguishable from a Poisson process with expected value $\lambda_\mathrm{r}\Delta t$ and variance $\lambda_\mathrm{r}\Delta t$. With increasing intervals Δt the occurrence of events within the intervals increases, the numbers $N(\Delta t)$ increasingly reflect variations expected from the distribution of wait times, and the variance $\mathrm{Var}[N(\Delta t)]$ converges to values expected for large times. This effect, that the occurrence of events is Poisson-like for small intervals Δt, is more pronounced with decreasing intensity λ_r. Note also that the variance may fall above or below the expected value depending on the ratio σ_w^2/μ_w^2; and if wait times are exponentially distributed such that $\sigma_w^2/\mu_w^2 = 1$, then $\lambda_\mathrm{r} = \lambda$ is the rate of a Poisson process. If the process is compounded, then the expected values and variances are displaced upward like a compound Poisson process (Figure 6.6).

In turn the variance of the particle flux $\mathrm{Var}[q_{nx}(\Delta t)] = (\sigma_w^2/\mu_w^2)\lambda_\mathrm{r}/\Delta t$ and the coefficient of variation is (Figure 6.7)

$$C_{q_{nx}} = \frac{\sigma_w}{\mu_w}\frac{1}{\sqrt{\lambda_\mathrm{r}\Delta t}}\,. \tag{6.32}$$

If the distribution $f_w(w)$ of wait times gives $\sigma_w^2/\mu_w^2 > 1$ (for example, a Weibull distribution with shape parameter $\alpha < 1$) then the coefficient of variation converges to zero more slowly than in the case of a Poisson process (Figure 6.5). If $\sigma_w^2/\mu_w^2 < 1$ (a Weibull distribution with $\alpha > 1$) then it converges

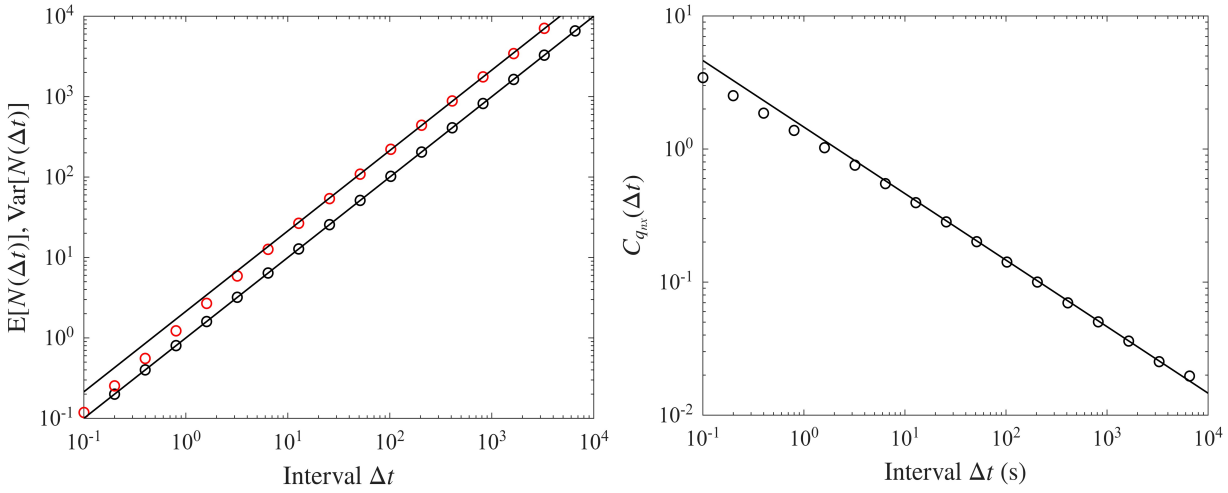

Figure 6.7: Plot of (left) expected value $\mathrm{E}[N(\Delta t)]$ and variance $\mathrm{Var}[N(\Delta t)]$ of the number $N(\Delta t)$ versus time interval Δt for a homogeneous Weibull renewal process (shape parameter $\alpha = 0.7$) with intensity $\lambda_\mathrm{r} = 1\ \mathrm{s}^{-1}$ together with synthetically generated expected values (black circles) and variances (red circles); and plot of (right) coefficient of variation $C_{q_{nx}}$ of the flux q_{nx} versus time interval Δt together with synthetically generated values (circles).

faster. Also recall that a Weibull process with shape parameter $\alpha < 1$ is equivalent to a Cox process (Yannaros, 1994) and yields bursty time series of events.

The properties described above lead to a key point. For homogeneous conditions the expected number $\mathrm{E}[N(\Delta t)]$ and the variance $\mathrm{Var}[N(\Delta t)]$ increase linearly with the time interval Δt. For a Poisson process the expected number and the variance are equal. For a compound Poisson process the variance is larger than the expected value, and for a simple renewal process the variance may be larger or smaller than the expected value depending on the form of the distribution of wait times (Figure 6.7). (As described in Chapter 12, this information helps constrain the form of possible distributions of wait times w.) In all cases the variance of the flux decreases as $\sim (\Delta t)^{-1}$ and the coefficient of variation decreases as $\sim (\Delta t)^{-1/2}$. Thus, whereas for a compound Poisson or renewal process the rate of convergence is modulated by the compounding distribution or the variance of wait times, these factors do not change the time dependence of the convergence. This means that the intensity of particle excitation — the entrainment rate E_n — leading to the value of λ, λ_c or λ_r is the principal factor controlling, indeed limiting, the convergence of estimates of the flux to the ensemble expected value. We illustrate this key point in later chapters. Meanwhile we now turn to unsteady conditions.

Inhomogeneous Conditions

Focusing on the examples of rain splash transport and bed load transport, both generally involve unsteady conditions at many time scales. Rain splash transport varies with changing rainfall intensity and storm frequency, and bed load transport varies with changing flow and streambed configurations. In Chapter 11 we show how the magnitude and uncertainty of the particle flux due to rain splash is influenced by unsteady rainstorm conditions. In Chapter 12, focused on bed load transport, we show that with complex rearrangements of the bed-surface texture during transport of a gravel mixture, some particle sizes exhibit unsteady transport despite fixed (steady) controlling factors. As one example, the experiments reported by Li et al. (2023) involve a mixture of two sizes ($D = 1$ mm and $D = 3$ mm) and clearly exhibit unsteady transport conditions as illustrated in their Figures 12a and 13.

Recall from Chapter 4 that, for an inhomogeneous Poisson process with time varying intensity

$\lambda(t)$, the number of events $N(t)$ occurring within an interval $(0,t]$ is a Poisson random variable with expectation,

$$\Lambda(t) = \int_0^t \lambda(t')\,\mathrm{d}t'\,. \tag{6.33}$$

That is, $\mathrm{E}[N(t)] = \mathrm{Var}[N(t)] = \Lambda(t)$. Notice that we may replace this with a time average, namely, $\Lambda(t) = \overline{\lambda}t$. Thus, $\mathrm{E}[N(t)] = \mathrm{Var}[N(t)] = \overline{\lambda}t$.

Consider a total interval of time T consisting of n non-overlapping intervals of length Δt such that $T = n\Delta t$. Then $\Lambda(T) = \overline{\lambda}T$ and likewise $\Lambda_i(\Delta t) = \overline{\lambda}_i\Delta t$, where $\overline{\lambda}_i$ is the average rate over the ith interval. That is, the number of events $N(\Delta t)$ in each interval of length Δt is described by a Poisson distribution $p_{Ni}(N;\overline{\lambda}_i,\Delta t)$ with expected value $\Lambda_i(\Delta t) = \overline{\lambda}_i\Delta t$ and variance $\Lambda_i(\Delta t) = \overline{\lambda}_i\Delta t$. The number of events $N(\Delta t)$ in the set of n intervals is then described by a mixture distribution $p_N(N;\Delta t)$ consisting of n Poisson distributions. That is,

$$p_N(N;\Delta t) = \frac{1}{n}\sum_{i=1}^{n} p_{Ni}(N;\overline{\lambda}_i,\Delta t)\,, \tag{6.34}$$

where the ratio $1/n$ indicates that the intervals of length Δt are equally weighted. Here it is important to appreciate that $p_N(N;\Delta t)$ is the *ensemble* distribution of all possible realizations $N(\Delta t)$ consisting of the equally weighted ensemble of all possible realizations $N(\Delta t)$ in each of the n intervals. We now want to know the expected value and the variance of this distribution as these vary with the interval Δt. Before proceeding, note that if the rate $\lambda(t) \to \lambda$ is fixed, then the distribution $p_N(N;\Delta t)$ just becomes the Poisson distribution $p_N(N;\lambda,\Delta t)$.

We can obtain expressions for the moments of the mixture distribution $p_N(N,\Delta t)$ using (2.87) and (2.88) from Chapter 2. For clarity, here we explicitly show the necessary calculations. The expected value is

$$\begin{aligned}
\mathrm{E}[N(\Delta t)] &= \sum_{N=0}^{\infty} N p_N(N;\Delta t) \\
&= \frac{1}{n}\sum_{i=1}^{n}\sum_{N=0}^{\infty} N p_{Ni}(N;\overline{\lambda}_i,\Delta t) \\
&= \frac{1}{n}\sum_{i=1}^{n}\langle N\rangle_i = \frac{1}{n}\sum_{i=1}^{n}\overline{\lambda}_i\Delta t = \overline{\lambda}\Delta t\,,
\end{aligned} \tag{6.35}$$

where angle brackets denote an average over the ith interval. Note that the last sum in (6.35) gives

$$\sum_{i=1}^{n}\Lambda_i(\Delta t) = \Lambda(T) = \overline{\lambda}T\,, \tag{6.36}$$

with $T = n\Delta t$. That is, the sum of the expected values of the intervals must sum to the expected value of the entire series of length T. These results indicate that the expected number $\mathrm{E}[N(\Delta t)]$ increases linearly with the time interval Δt at a rate equal to the average rate $\overline{\lambda}$.

The variance $\mathrm{Var}[N(\Delta t)]$ of the number $N(\Delta t)$ is

$$\begin{aligned}
\mathrm{Var}[N(\Delta t)] &= \sum_{N=0}^{\infty} N^2 p_N(N;\Delta t) - \left(\mathrm{E}[N(\Delta t)]\right)^2 \\
&= \frac{1}{n}\sum_{i=1}^{n}\sum_{N=0}^{\infty} N^2 p_{Ni}(N;\overline{\lambda}_i,\Delta t) - \overline{\lambda}^2(\Delta t)^2\,.
\end{aligned} \tag{6.37}$$

This leads to

$$\mathrm{Var}[N(\Delta t)] = \frac{1}{n}\sum_{i=1}^{n}\left\langle N^2\right\rangle_i - \overline{\lambda}^2(\Delta t)^2\,. \tag{6.38}$$

Note that $\left\langle N^2\right\rangle_i = \overline{\lambda}_i\Delta t + \overline{\lambda}_i^2(\Delta t)^2$ so

$$\mathrm{Var}[N(\Delta t)] = \frac{1}{n}\sum_{i=1}^{n}\left[\overline{\lambda}_i\Delta t + \overline{\lambda}_i^2(\Delta t)^2\right] - \overline{\lambda}^2(\Delta t)^2\,. \tag{6.39}$$

This gives

$$\begin{aligned}\mathrm{Var}[N(\Delta t)] &= \overline{\lambda}\Delta t + \left(\left\langle\!\left\langle \overline{\lambda}_i^2\right\rangle\!\right\rangle - \overline{\lambda}^2\right)(\Delta t)^2 \\ &= \overline{\lambda}\Delta t + \mathrm{V}_\lambda(\Delta t)(\Delta t)^2\,,\end{aligned} \tag{6.40}$$

where double angle brackets denote an average over the n intervals so that $\mathrm{V}_\lambda(\Delta t) = \left\langle\!\left\langle \overline{\lambda}_i^2\right\rangle\!\right\rangle - \overline{\lambda}^2$ is the variance of the n values of the rate $\overline{\lambda}_i$.

As written, the expected value $\mathrm{E}[N(\Delta t)]$ given by (6.35), and the variances $\mathrm{Var}[N(\Delta t)]$ and $\mathrm{V}_\lambda(\Delta t)$ given by (6.40), are very general. These are agnostic to the specific structure of the intensity $\lambda(t)$, which may be monotonic or non-monotonic. To illustrate this point we consider two cases. The first is when the intensity $\lambda(t)$ varies linearly, increasing or decreasing, over a finite period T, and the second case is when $\lambda(t)$ varies as a sinusoidal function, as suggested by particle flux signals presented in Chapter 12.

For the linear case, let $T = n\Delta t$ denote the total sampling period involving n intervals of length Δt. We then assume that $\lambda(t) = b_0 + b_1 t$ for $0 \le t \le T$, where b_0 is the starting rate $\lambda(0)$ at time $t = 0$ and b_1 is the rate of change in $\lambda(t)$. The variance $\mathrm{V}_\lambda(\Delta t)$ is then (Appendix D)

$$\mathrm{V}_\lambda(\Delta t) = \frac{b_1^2}{12}\left[T^2 - (\Delta t)^2\right]\,. \tag{6.41}$$

In turn the variance of $N(\Delta t)$ becomes

$$\mathrm{Var}[N(\Delta t)] = \overline{\lambda}\Delta t + \frac{b_1^2}{12}\left[T^2 - (\Delta t)^2\right](\Delta t)^2\,. \tag{6.42}$$

Thus, the variance $\mathrm{Var}[N(\Delta t)]$ systematically increases with increasing interval Δt then goes to $\mathrm{E}[N(T)] = \overline{\lambda}T$ in the limit of $\Delta t \to T$ (Figure 6.8). This result occurs for positive or negative change of rate b_1.

Consider a sinusoidal signal, where it is convenient to choose a cosine function. The ensemble of possible realizations is defined by $\lambda(t) = \lambda_0 + A\cos(\omega t + \phi)$ with average rate λ_0, amplitude A, angular frequency $\omega = 2\pi/T_\lambda$ for period T_λ, and uniformly distributed phase $\phi = \mathrm{U}(-\pi \le \phi \le \pi)$. Because this signal is strictly stationary, the phase does not influence the ensemble expected values. For simplicity we therefore choose $\phi = 0$ so that $\lambda(t) = \lambda_0 + A\cos(\omega t)$. Note also that the results are insensitive to a nonzero phase ϕ for a finite interval T so long as T spans a large proportion of the period T_λ (Appendix D). The variance $\mathrm{V}_\lambda(\Delta t)$ is given by

$$\mathrm{V}_\lambda(\Delta t) = \frac{A^2}{\omega^2(\Delta t)^2}[1 - \cos(\omega\Delta t)]\,. \tag{6.43}$$

In turn the variance of $N(\Delta t)$ becomes

$$\mathrm{Var}[N(\Delta t)] = \lambda_0\Delta t + \frac{A^2}{\omega^2(\Delta t)^2}[1 - \cos(\omega\Delta t)](\Delta t)^2\,. \tag{6.44}$$

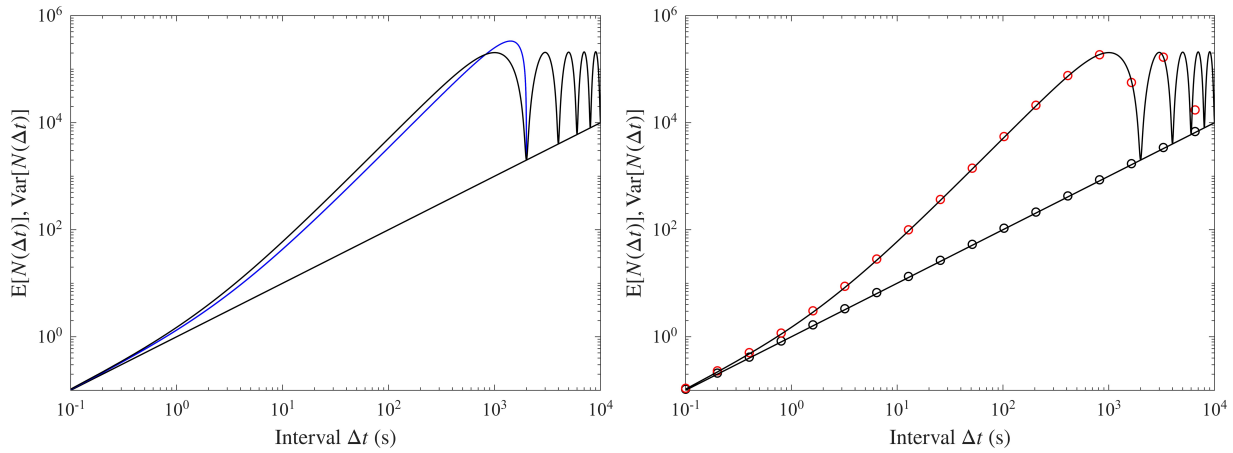

Figure 6.8: Plots of (left) expected value $\mathrm{E}[N(\Delta t)]$ (straight line) and variance $\mathrm{Var}[N(\Delta t)]$ of the number $N(\Delta t)$ versus time interval Δt for (blue line) linear variation in rate $\lambda(t)$ over interval $T = 2\,000$ s and (black line) sinusoidal variations in rate $\lambda(t)$ with period $T_\lambda = 2\,000$ s; and (right) plot of sinusoidal case together with synthetically generated expected values (black circles) and variances (red circles).

Thus, the variance $\mathrm{Var}[N(\Delta t)]$ systematically increases with increasing Δt then oscillates above the expected value with fixed amplitude and period with frequency $1/T_\lambda$ for $\Delta t \geq T_\lambda$ (Figure 6.8).

For later reference, consider a signal $\lambda(t)$ composed of m independent harmonics with amplitudes A_j and angular frequencies ω_j. A straightforward derivation (Appendix D) gives

$$\mathrm{V}_\lambda(\Delta t) = \sum_{j=1}^{m} \frac{A_j^2}{\omega_j^2 (\Delta t)^2} [1 - \cos(\omega_j \Delta t)] \,. \tag{6.45}$$

The variance of $N(\Delta t)$ becomes

$$\mathrm{Var}[N(\Delta t)] = \lambda_0 \Delta t + \sum_{j=1}^{m} \frac{A_j^2}{\omega_j^2 (\Delta t)^2} [1 - \cos(\omega_j \Delta t)] (\Delta t)^2 \,. \tag{6.46}$$

With a mixture of periods and phases the variance $\mathrm{Var}[N(\Delta t)]$ generally remains larger than the expected value $\mathrm{E}[N(\Delta t)]$ at large Δt.

Focusing on the variances given by (6.40), in general the variance $\mathrm{V}_\lambda(\Delta t)$ is a maximum in the limit of $\Delta t \to 0$ then monotonically decreases with increasing interval Δt (Figure 6.9). Nonetheless, with small time intervals Δt the variance $\mathrm{Var}[N(\Delta t)]$ increases nearly linearly, then the quadratic term in (6.40) dominates with increasing Δt (Figure 6.8). This occurs for both the linear and sinusoidal functions $\lambda(t)$. This hand off from the linear term with small intervals Δt to the nonlinear term with increasing intervals can be explained as follows. For small intervals Δt the variance $\mathrm{Var}[N(\Delta t)]$ is sensitive to chance differences in the sets of wait times between events and the associated numbers $N(\Delta t)$ within the n intervals. Despite different rates $\overline{\lambda}_i$ across the n intervals, these intervals are sufficiently small that most of them contain no events or only one event. The mixture distribution $p_N(N; \Delta t)$, representing mostly zeros, is indistinguishable from a Poisson distribution with expected value $\overline{\lambda} \Delta t$. This represents the intermittent stage defined by Ma et al. (2014). With increasing intervals Δt, variations in the numbers $N(\Delta t)$ are due less to chance differences in the sets of wait times and more to differences in the average rates $\overline{\lambda}_i$ over the n intervals due to fluctuations in the numbers of crossing events as reflected by the variance $\mathrm{V}_\lambda(\Delta t)$. This represents the invariant stage described by Ma et al. (2014). As described further below and in Chapter 12, the nonlinear variation

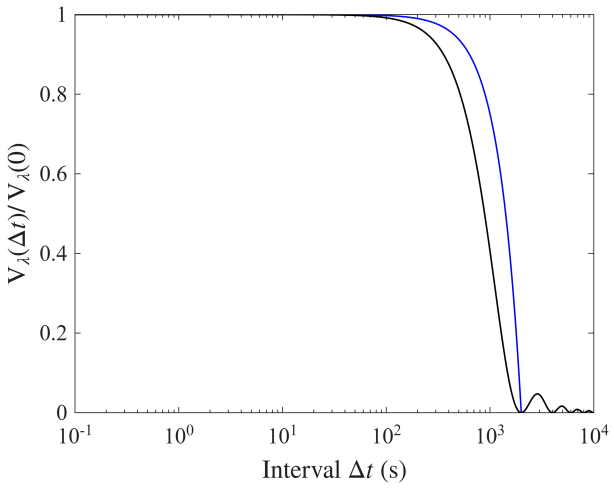

Figure 6.9: Plot of variance $V_\lambda(\Delta t)$ for (blue line) linear variation in rate $\lambda(t)$ over interval $T = 2\,000$ s and (black line) sinusoidal variation in rate $\lambda(t)$ with period $T_\lambda = 2\,000$ s, both normalized by variance $V_\lambda(0)$.

of $\mathrm{Var}[N(\Delta t)]$ in Figure 6.8 for these two stages is insensitive to the specific structure of the rate $\lambda(t)$. With large intervals Δt, however, the specifics of $\lambda(t)$ matter.

Specifically, the functional form of the variance $V_\lambda(\Delta t)$ depends on the structure of $\lambda(t)$ (Figure 6.9) and this becomes manifest at large intervals Δt. If $\lambda(t)$ is a linear function over a total time $T = n\Delta t$ then $V_\lambda(\Delta t)$ is quadratic in Δt such that the variance $\mathrm{Var}[N(\Delta t)]$ necessarily returns to the expected value $\mathrm{E}[N(\Delta t)]$ in the limit of $\Delta t \to T$ (Figure 6.8). If $\lambda(t)$ is a strictly stationary sinusoid then $V_\lambda(\Delta t)$ is a cosine function such that the variance $\mathrm{Var}[N(\Delta t)]$ oscillates above the expected value $\mathrm{E}[N(\Delta t)]$ with fixed period (Figure 6.8). If $\lambda(t)$ is a stationary mixture of sinusoids then the variance $\mathrm{Var}[N(\Delta t)]$ remains above the expected value with magnitude reflecting the total variance of the mixture. In the analysis of Ma et al. (2014) the rate $\lambda(t)$ is treated as a stochastic rather than deterministic process such that the variance $\mathrm{Var}[N(\Delta t)]$ grows linearly with large Δt in a Poissonian manner, albeit at a rate larger than the expected rate $\overline{\lambda}$.

We also can write the coefficient of variation of the flux, $C_{q_{nx}}(\Delta t)$. For a linear variation in $\lambda(t)$ over the total period T,

$$C_{q_{nx}}(\Delta t) = \frac{1}{\sqrt{\overline{\lambda}\Delta t}} \sqrt{1 + \frac{b_1^2 \Delta t}{12\overline{\lambda}} \left[T^2 - (\Delta t)^2\right]} \,. \tag{6.47}$$

For a sinusoidal variation in $\lambda(t)$,

$$C_{q_{nx}}(\Delta t) = \frac{1}{\sqrt{\lambda_0 \Delta t}} \sqrt{1 + \sum_{j=1}^{m} \frac{A_j^2}{\lambda_0 \omega_j^2 \Delta t} [1 - \cos(\omega_j \Delta t)]} \,. \tag{6.48}$$

These results have important implications for assessing the uncertainty of time-averaged estimates of the particle flux. With inhomogeneous conditions, convergence may not occur with increasing intervals Δt. The uncertainty measured by $C_{q_{nx}}$ for a specific averaging interval Δt can be much larger than that associated with homogeneous conditions at large Δt (Figure 6.10). Thus, achieving a specific level of uncertainty might require long averaging times. It is possible to generalize this result to other processes, for example, an inhomogeneous compound Poisson or a simple renewal process (Chapter 12).

The developments above describe ensemble conditions whereas normally we have a single experimental time series. Nonetheless, because intervals of length Δt are non-overlapping we can straightaway

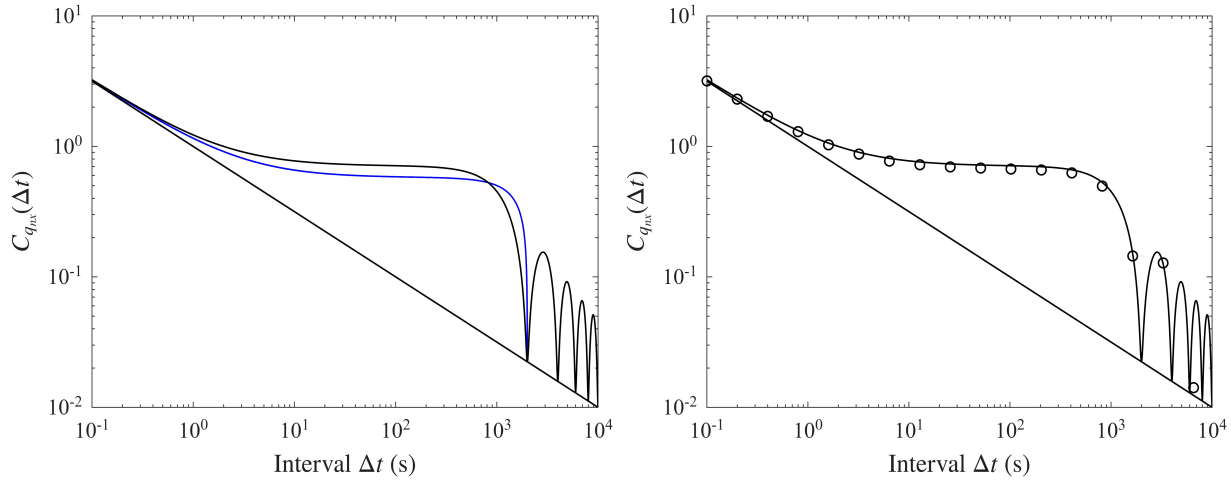

Figure 6.10: Plot of (left) coefficient of variation $C_{q_{nx}}(\Delta t)$ of the particle number flux q_{nx} versus time interval Δt for (blue line) linear variation in rate $\lambda(t)$ over interval $T = 2\,000$ s and (black line) sinusoidal variation in rate $\lambda(t)$ with period $T_\lambda = 2\,000$ s, where black straight line represents coefficient of variation for a homogeneous Poisson process with rate equal to the average $\overline{\lambda}$; and (right) plot of sinusoidal case together with synthetically generated values (circles).

estimate values of $\mathrm{E}[N(\Delta t)]$ and $\mathrm{Var}[N(\Delta t)]$ for a sufficiently long experimental series (Ma et al., 2014; Allen, 2023; Li et al., 2023; Chapter 12). In effect this is occurring with the synthetic series presented in the figures above. Confidence in the estimates necessarily decrease with large Δt as the number n of intervals decreases.

As elaborated in Chapter 11, whereas raindrop impacts are Poisson in space and time, the time series of the number of entrained particles is a compound Poisson process, as is the time series of the number of particles that cross a specified coordinate position. In addition the expectation given by (6.35) is particularly relevant to unsteady conditions of rain splash transport where for typical rainfall intensities the convergence of realizations of the particle flux to an ensemble expected value cannot occur over rainstorm time scales. Similarly, we may in the simplest case envision entrainment of bed load particles as being Poisson in space and time (Einstein, 1950), although in detail this likely is more complicated with effects of turbulence structures and collective entrainment (e.g. Roseberry et al., 2012; Heyman et al., 2013; Ancey and Heyman, 2014; Ma et al., 2014; Fathel et al., 2015; Lee and Jerolmack, 2018; see Chapter 12). Owing to randomization effects of finite travel times with displacements, the form of the distribution of wait times associated with crossing events may not match that of the entrainment events. We show in Chapter 12 that crossing events of relatively coarse gravel particles are consistent with a Poisson process, and that the time series of smaller gravel particles are consistent with inhomogeneous conditions, likely involving a simple compound or renewal process. The results depicted in Figures 6.5, 6.6, 6.7 and 6.8 provide particularly useful diagnostics for interpreting the experimental times series of bed load particle transport.

6.4.2 Moving Average

In the literature the local particle flux often is straightaway treated as a deterministic continuum-like quantity, particularly when used with the Exner equation, without reference to time averaging or spatial resolution. This notably includes work on the initial instability and formation of bedforms (see reviews by: Nelson, 1990; Charu et al., 2013; Andreotti and Claudin, 2015; Bohorquez et al., 2025) and descriptions of rill and gully development on hillslopes in response to surface flows and rain splash transport (e.g. McGuire et al., 2013; Hancock and Willgoose, 2021). This practice hinges

on curious — indeed contradictory — reasoning because deterministic semi-empirical formulations of the flux as embodied in (1.6) or (1.7) invariably are experimentally calibrated and tested with time-averaged values of the flux, as such averaging is necessary to provide convergence to steady (deterministic-like) values which are then related functionally to selected controlling factors (e.g. the bed stress). Based on conversations with colleagues, some researchers acknowledge the particle flux is a time-averaged quantity with uncertainty, then use it in a deterministic manner by conceptualizing it as a moving average analogous to what we might envision in appealing to a Reynolds-averaged flow velocity, albeit without reference to the spatial resolution involved. We thus turn to the consequences of this conceptualization of the particle flux for rarefied conditions, focusing on bed load, with specific relevance to interpretations of the Exner equation (Chapters 7 and 13).

For a specified resolution Δy or Δx the time average over an interval Δt in (6.4) or (6.5) can be reinterpreted as a moving average. Physical interpretability suggests that we should look backward in time, and we therefore rewrite (6.4) as

$$q_{nx}(t;\Delta t) = \frac{1}{\Delta y \Delta t}\int_{t-\Delta t}^{t} I(t';\Delta y)\,\mathrm{d}t' \,. \tag{6.49}$$

In this view the flux evaluated at time t represents an arithmetically weighted memory of previous crossing events, where the appearance of Δt in the functional notation highlights the dependence on this selected (fixed) interval. Now the problem becomes one of signal analysis. Here we highlight essential consequences with examples, noting the similarity with the smoothing of experimental data performed by Li et al. (2023).

The time averaging in (6.49) represents a low-pass filter. The effect of increasing Δt is to increasingly suppress higher frequency fluctuations and pass lower frequency variations. A nominally instantaneous estimate of the flux at time t is replaced with an average over previous times to $t - \Delta t$. If for fixed controlling factors (flow, flow depth, water-surface slope, sediment properties and so on) the interval Δt is sufficiently large that convergence of the flux q_{nx} to a value with small uncertainty occurs, then presumably this is a good estimate of the expected value $\langle q_{nx}\rangle$ to go with the specified controlling factors. With small Δt, however, the estimate given by (6.49) merely represents an outcome associated with the variability in the numbers of crossings of a particular realization, and not the value that we might deterministically expect for the imposed conditions.

Consider statistically steady transport. For simplicity of illustration we choose a Weibull renewal process with rate $\lambda_\mathrm{r} = \langle q_{nx}\rangle \Delta y$. As described above (Section 6.4.1) the standard deviation of the set of realizations about the expected value is $(\sigma_w/\mu_w)\sqrt{\lambda_\mathrm{r}}/\sqrt{\Delta t}$ and the coefficient of variation $C_{q_{nx}} = (\sigma_w/\mu_w)/\sqrt{\lambda_\mathrm{r}\Delta t}$. Thus,

$$\Delta t = \frac{\sigma_w^2/\mu_w^2}{C_{q_{nx}}^2 \lambda_\mathrm{r}} = \frac{\sigma_w^2/\mu_w^2}{C_{q_{nx}}^2 \langle q_{nx}\rangle \Delta y} \tag{6.50}$$

is the averaging interval required to achieve a particular level of uncertainty represented by the value of $C_{q_{nx}}$. This highlights the role of the spatial resolution represented by the length Δy. For example, a rate $\lambda_\mathrm{r} = 1\ \mathrm{s}^{-1}$ could be associated with an expected flux $\langle q_{nx}\rangle = 1\ \mathrm{m}^{-1}\ \mathrm{s}^{-1}$ with $\Delta y = 1$ m, or an expected flux $\langle q_{nx}\rangle = 10\ \mathrm{m}^{-1}\ \mathrm{s}^{-1}$ with $\Delta y = 0.1$ m, and so on.

With $\lambda_\mathrm{r} = 2\ \mathrm{s}^{-1}$, a value that is consistent with measurements of gravel transport reported by Chartrand (2017), the estimated rate $q_{nx}\Delta y$ fluctuates significantly about the expected value for small averaging intervals Δt (Figure 6.11). A flux signal that we might consider as being reasonably smooth emerges only with $\Delta t = 1\,000$ s ($\approx$ 17 minutes) with $C_{q_{nx}} \approx 0.03$. As indicated by (6.50), for an uncertainty specified by $C_{q_{nx}}$ the rate of convergence increases with increasing rate λ_r.

Consider unsteady conditions in which the expected rate λ_r increases linearly with time (Figure 6.12). As with the example above involving a fixed rate, the estimated flux fluctuates significantly about the expected value for small averaging intervals Δt. In addition, because the expected value is

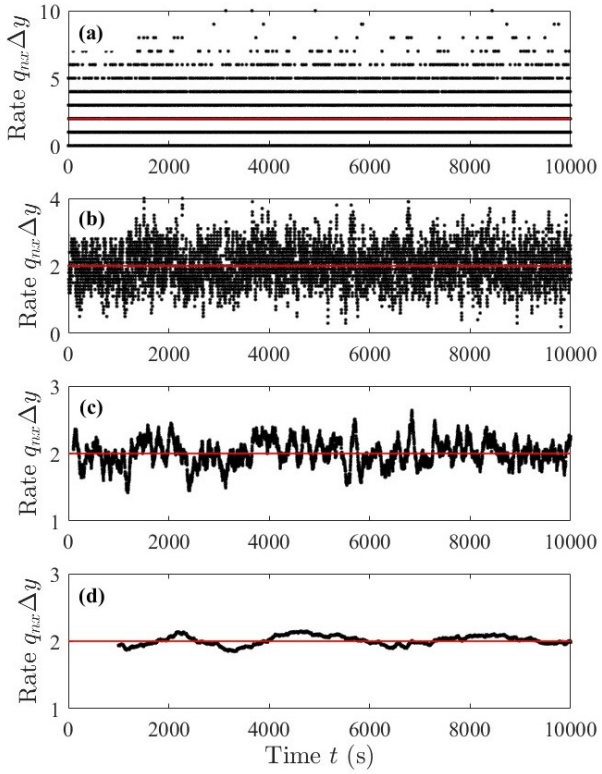

Figure 6.11: Plot of rate $q_{nx}\Delta y$ with expected rate $\lambda_\mathrm{r} = \langle q_{nx}\rangle \Delta y = 2\ \mathrm{s}^{-1}$ (red line) for **(a)** $\Delta t = 1$ s, $C_{q_{nx}} = 0.89$, **(b)** $\Delta t = 10$ s, $C_{q_{nx}} = 0.28$, **(c)** $\Delta t = 100$ s, $C_{q_{nx}} = 0.089$, **(d)** $\Delta t = 1\,000$ s, $C_{q_{nx}} = 0.028$ with $\sigma_w/\mu_w = 1.26$.

continuously changing, the moving average can never converge. The averaging is aimed at a moving target and the averaged flux mostly lags the expected flux. This becomes increasingly pronounced with an increasing rate of change in λ_r. In this example the moving average in effect is an estimate of the average rate $\overline{\lambda}_\mathrm{r}$ for the preceding interval Δt, as described in Section 6.4.1.

Note that this linear variation in the rate λ_r (Figure 6.12) is essentially the increasing part of a sinusoid with a much longer period. We show in Appendix D that, as a one-sided low-pass filter, (6.49) has the effect of attenuating the amplitude of a sinusoidal signal and adding a phase shift relative to the expected rate. This effect becomes pronounced when the averaging interval Δt approaches the period of the signal.

These points lead to the idea of quasi-steady conditions. We start by defining a characteristic time scale of change in the expected rate λ,

$$T_\lambda = \frac{\lambda}{\mathrm{d}\lambda/\mathrm{d}t}\,. \tag{6.51}$$

If the averaging interval $\Delta t \ll T_\lambda$, then we may assume that quasi-steady conditions exist. However, the interval Δt must be sufficiently large to achieve a desired degree of convergence, thus requiring a compromise. Whereas a short averaging interval gives large uncertainty about the expected rate, a long averaging interval might give small apparent uncertainty, but it cannot resolve the expected rate if this rate changes over a time scale T_λ that is on the same order or shorter than the averaging interval Δt.

Returning to the conceptualization of the expected flux as a moving average, unless experimental measurement techniques allow it, we do not observe the fluctuating, albeit smoothed, time series in Figure 6.11 and Figure 6.12 representing an example of actual conditions. Meanwhile, the solid

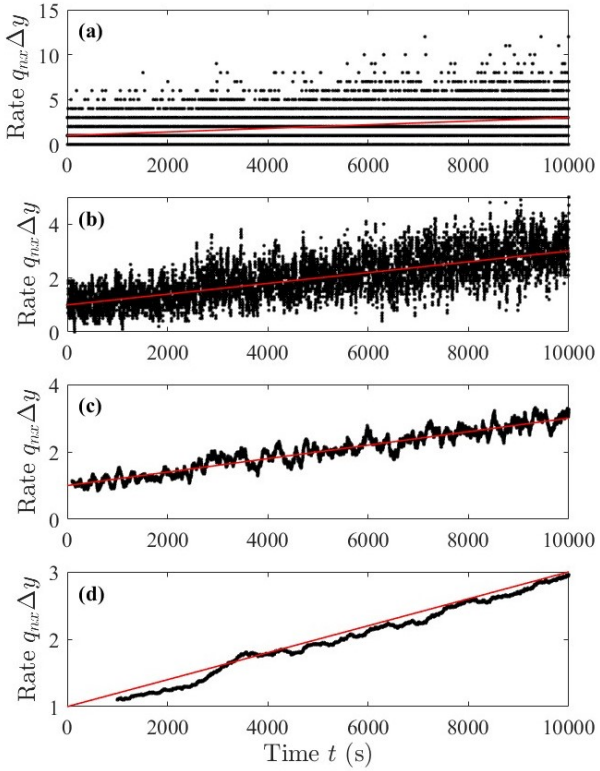

Figure 6.12: Plot of rate $q_{nx}\Delta y$ with expected rate $\lambda_r = \langle q_{nx}\rangle \Delta y$ that increases linearly (red line) for **(a)** $\Delta t = 1$ s, **(b)** $\Delta t = 10$ s, **(c)** $\Delta t = 100$ s, **(d)** $\Delta t = 1\,000$ s.

line is what we might *imagine* is occurring based on a deterministic prediction of the transport rate for specific controlling factors at any instant, assuming this expectation is unique to these factors. (Uniqueness is reasonable for rain splash transport, but is questionable for bed load transport; see Chapter 12.) To conceptualize a deterministically specified value as a moving average does not imply that it coincides with actual conditions. With nominally steady transport it may represent, with uncertainty, time averaged conditions in the same sense that the logarithmic velocity law represents the Reynolds-averaged fluid velocity $\overline{u}(z)$ at a position z above the boundary. But the specified value does not represent what occurs at time t in any realization, just as the logarithmic velocity law says nothing about the instantaneous velocity $u(z,t)$ at z. With unsteady conditions the specified value might represent, with uncertainty, quasi-steady averaged conditions, but only if these change slowly relative to the averaging time. In this situation it might correctly "predict" averaged conditions at time $t + \delta t$ for small δt. But it most certainly cannot predict in a deterministic manner what occurs at time $t + \delta t$ in any realization.

Real time series of transport often exhibit fluctuations that are larger than those depicted in the idealized examples above (Figure 6.11 and Figure 6.12). With reference to Figure 6.10, and as illustrated in Chapter 12, with inhomogeneous transport conditions the uncertainty measured by $C_{q_{nx}}$ for a specific averaging interval Δt can be much larger than that associated with a simple renewal process as depicted in Figures 6.11 and 6.12.

6.5 Local Versus Nonlocal Transport

Nonlocal transport refers to the physical concept that attributes of particle motions used in defining the flux or its divergence at a position x depend on conditions "far" from this position. Local transport

then loosely refers to a mathematical concept, that the flux at a position x is expressed in terms of quantities that are evaluated locally at this position. To be clear, in this view of things local transport does not actually refer to a physical thing. Rather, it refers to the familiar idea of a local function, to mean that the flux depends only on quantities, and derivatives of these quantities, defined precisely (locally) at x. Indeed, these two points are readily illustrated by the entrainment form of the flux as embodied in (6.23) and (6.26), as follows.

According to (6.23) the expected flux $\langle q_{nx} \rangle$ at a position x explicitly depends on the rate of particle entrainment E_n at positions x' upslope or upstream of x, that is, involving conditions far from x that lead to entrainment. The expected flux also explicitly depends on the distribution of travel distances L_x and the exceedance probability function $R_{L_x|T_\mathrm{p}}$ conditioned on travel times T_p, again involving conditions far from x that set the form of this distribution and its moments — notably including the detailed statistical mechanics of particle–surface interactions that particles experience in moving from any position $x' = x - L_x$ to x. Thus, the integral form of (6.23) quintessentially represents a nonlocal description of the particle flux, in that particles contributing to the flux at x are mechanically influenced by conditions far from x, and this influence is integrated over all possible upslope or upstream starting positions.

Note, then, that when (6.23) is approximated as an advection–diffusion equation as in (6.26), this still implies the existence of the underlying nonlocal physical behavior as summarized above. Yet now we must concede that the advective and diffusive terms in (6.26) are mathematically *local* expressions, each evaluated at the position x. To emphasize this point we might choose to explicitly use the functional notation $E_n(x)$, $\langle L_x \rangle(x)$ and $\langle L_x^2 \rangle(x)$ and rewrite (6.26) as

$$\langle q_{nx}(x) \rangle = E_n(x) \langle L_x \rangle(x) - \frac{1}{2} \frac{\partial}{\partial x} \left[E_n(x) \langle L_x^2 \rangle(x) \right] \; . \tag{6.52}$$

To be clear, (6.52) is a mathematically local expression of transport that represents, as an approximation, the physical reality of nonlocal transport as embodied in the integral expression (6.23). In particular, we may view the diffusive term in (6.52) as registering information on how the entrainment rate or the raw variance of particle displacements, or both, vary in the vicinity of x (i.e. nonlocally), whence this term approximates the effects of these variations on the local flux at x.

A similar perspective pertains to the advective and diffusive terms of the activity form of the particle flux given by (6.16). Namely, we show in Chapter 7 that (6.16) derives as an approximation of a nonlocal integral expression analogous to (6.23). We might then use functional notation and rewrite (6.16) as

$$\langle q_{nx}(x) \rangle = \langle \gamma_n \rangle(x) \langle v_x \rangle(x) - \frac{\partial}{\partial x} \left[\kappa(x) \langle \gamma_n \rangle(x) \right] \; , \tag{6.53}$$

thereby highlighting that the advective and diffusive terms are evaluated at the position x. Yet this mathematically local expression of transport represents the physical reality of nonlocal transport as embodied in a master equation — a convolution integral — describing the evolution of the probability distribution of particle positions (Chapter 7).

The idea of local versus nonlocal transport as summarized above is the view adopted throughout this book, namely, that sediment transport is effectively nonlocal when viewed from a physical perspective (Furbish et al., 2017b; Doane, 2018; Furbish and Doane, 2021). Nonetheless, different interpretations of local versus nonlocal transport have emerged in the literature, specifically in relation to particle transport on hillslopes and tracer particle motions in rivers (Schumer et al., 2009; Foufoula-Georgiou et al., 2010; Furbish and Haff, 2010; Furbish and Roering, 2013; Doane et al., 2018, 2019; Furbish et al., 2021a). This specifically echoes ideas centered on Lévy motions during transport in porous media as described using methods of fractional calculus (Benson et al., 2000, 2001; Schumer et al., 2003), thence adapted to descriptions of sediment tracer particles (e.g. Schumer et al., 2009).

To illustrate this point, let us start by taking the divergence of the activity form of the flux as described by (6.53) to give

$$\frac{\partial \langle \gamma_n \rangle}{\partial t} = -\langle v_x \rangle \frac{\partial \langle \gamma_n \rangle}{\partial x} + \kappa \frac{\partial^2 \langle \gamma_n \rangle}{\partial x^2} \,, \tag{6.54}$$

where for simplicity we are assuming a constant mean velocity and diffusivity, and we are neglecting source or sink terms (Chapter 7). Then suppose for comparison that the underlying distribution of particle displacements is heavy-tailed with undefined variance. Recall from Chapter 3 that the generalized central limit theorem leads to the possibility of anomalous diffusion, wherein the advection–diffusion equation describing the evolution of the distribution of particle positions $f_x(x,t)$ involves a fractional derivative. Namely,

$$\frac{\partial f_x(x) \rangle}{\partial t} = -\langle v_x \rangle \frac{\partial f_x(x,t)}{\partial x} + \kappa \frac{\partial^\alpha f_x(x,t)}{\partial x^\alpha} \,, \tag{6.55}$$

with $1 < \alpha \leq 2$ denoting the stability parameter of an α-stable distribution that represents superdiffusive particle spreading owing to the heavy-tailed form of the distribution of particle displacements. In this situation the fractional derivative operator $\mathrm{D}_x^\alpha = \partial^\alpha / \partial x^\alpha$ is nonlocal. It is symbolic, to mean a weighted integral evaluated over the domain of the function $f_x(x,t)$. Specifically, for a function $f(x)$ that is continuous over $(0, \infty)$, then one example is the Caputo derivative defined as

$$\mathrm{D}_x^\alpha f(x) = \frac{1}{\Gamma(n-\alpha)} \int_0^x \frac{f^{(n)}(z)}{(x-z)^{\alpha+1-n}} \, \mathrm{d}z \,, \tag{6.56}$$

with variable of integration z, where $n - 1 < \alpha < n \in \mathbb{N}$. If in contrast to an ordinary advection–diffusion equation we claim that (6.55) represents nonlocal transport as a consequence of the underlying presence of a heavy-tailed distribution of particle displacements (e.g. Schumer et al., 2009), then it becomes clear that this claim pertains to the mathematics — the nonlocal derivative operator — not to the physical phenomenon of transport. Indeed, from a physical perspective this purely mathematical distinction between local and nonlocal transport as decided by the form of the underlying distribution of particle displacements — light-tailed versus heavy-tailed — is arbitrary.

To wit, consider the example in which particle displacements $r \geq 0$ on a hillslope (Chapter 10) are described by a generalized Pareto distribution $f_r(r; A, B)$ with shape parameter A and scale parameter B. Recall from Chapter 2 that when $A = 0$ this distribution reduces to an exponential distribution. When $A < 0$ this distribution is bounded at $r = B/|A|$. When $A \geq 1/2$ the variance is undefined, and when $A \geq 1$ the mean is undefined. As described in Chapter 10, the generalized Pareto distribution reflects the statistical physics of particle disentrainment in which, following entrainment, the cessation of motion within any interval downslope is probabilistic. The form and parametric values of the distribution reflect the energetics of particle–surface collisions during downslope movement, specifically the balance between the particle kinetic energy gained from gravitational potential energy and the extraction of kinetic energy by collisions.

Now consider the mechanical conditions associated with values of $\pm A$ infinitesimally close to $A = 0$ separating bounded and heavy-tailed forms of $f_r(r; A, B)$. In fact, there are no meaningful differences in the detailed statistical mechanics of particle motions associated with these different values of $\pm A$ (Furbish et al., 2021c; Furbish and Doane, 2021). And, in practical terms the two conditions would be statistically indistinguishable. Similarly, there are no meaningful (measurable) differences in the statistical mechanics of particle motions associated with the transition marked by $A = 1/2$ at which the variance of the distribution $f_r(r; A, B)$ is defined or undefined. In other words, all situations involve nonlocal transport when viewed from a physical perspective, such that a distinction between local and nonlocal transport based on the mathematical form of the distribution $f_r(r)$ is arbitrary. Moreover, we reach identical conclusions for bed load transport when considering the essential role of the detailed

statistical mechanics of particle–bed collisions that contribute to variations in the distributions of particle velocities and hop distances (Chapter 12).

Recall that the starting point of this chapter — our description of the particle flux as a counting process (Section 6.2.1) — together with our descriptions of the activity and entrainment forms of the flux (Section 6.3) refers to specific processes, for example, rain splash and bed load transport, and thus to the spatial scales inherent to these processes. Nonetheless, the derived kinematic expressions are in fact agnostic to scale. That is, the expressions of the particle number flux — (6.3), (6.4) and (6.5) — and the expressions of the expected flux — (6.16) and (6.26) — are all independent of scale. With reference to Figure 6.1, the depiction of particles crossing the control surface A could represent the scale of atoms in a gas, or equally, the scale of coarse gravel exiting a flume. As a consequence, when viewed at the scale of particle motions the physical idea of nonlocal transport as embodied in the various expressions of the particle flux is scale independent.

To illustrate this point at the smallest relevant scale, consider an elementary area A located at a coordinate position x within a continuum fluid through which particles are moving. A particle that crosses A at time t with velocity v_x is counted as part of the flux of particles through A. Such a particle started its motion toward A from a collision with another particle at a distance, on average, equal to the mean free path. Of course, particles that cross A during a small interval $\mathrm{d}t$ started their motions from collisions at distances smaller than and larger than the mean free path. Nonetheless, inasmuch as particle transport is characterized by the particle flux through A, we must conclude that the particle velocities contributing to this flux during $\mathrm{d}t$ are determined by collisions with other particles "far" from A. Indeed, choosing air at normal pressure–temperature conditions, the mean free path is about 10^3 larger than the effective particle diameter. If we imagine a soccer ball as an air molecule, then it went into the goal after traveling a distance, on average, equal to twice the length of the soccer field. Viewed from a physical perspective, the particle flux at A therefore is the outcome of decidedly nonlocal particle–particle interactions. When we back out to the Knudsen scale where we no longer see the particles, the continuum flux at a position x becomes a local mathematical expression — the product of the average particle velocity and the number concentration. This is afforded by continuum conditions; but the detailed particle kinematics contributing to the flux are nonetheless nonlocal when viewed at the scale of particle motions.

To reinforce this point, consider tracer particles within a continuum fluid. The behavior of the particles is described by an ordinary advection–diffusion equation involving Fickian diffusion. This equation is obtained from a master equation whose integral form is essentially the same as that used in describing conservation of sediment particles (Chapter 7) leading to the advection–diffusion equation (6.54). Moreover, as in the description above regarding sediment particle diffusion, the local derivative $\partial c(x,t)/\partial x$ of the concentration $c(x,t)$ of tracer particles, as it appears in Fick's first law, registers information on how the number of tracer particles varies in the vicinity of the position x (i.e. nonlocally), and approximates the effects of this variation on the local flux at x. Then, anomalous diffusion at this molecular scale is something that is not Fickian, perhaps due to a difference in the distribution of particle velocities, but it is no more nonlocal from a physical perspective than is Fickian diffusion.

For completeness let us note that ideas of locality also appear in granular physics in relation to nonlocal effects in the rheological behavior of dense granular materials during creep and flow (Pouliquen and Forterre, 2009; Kamrin and Koval, 2012; Henann and Kamrin, 2013; Bouzid et al., 2015; Tang et al., 2018; Fazelpour and Daniels, 2023). For example, one can envision that local particle–particle contact forces and interactions during bulk strain may be influenced nonlocally inasmuch as forces can be transmitted over relatively large distances via granular force chains and their networks. In this vein, Pouliquen and Forterre (2009) conceptualize local particle rearrangements as a self-activated process during shear, such that a "rearrangement at one position is triggered by the stress fluctuations induced by rearrangements elsewhere in the material... [whence] the constitutive law, which gives the relation between the shear rate and the stress distribution, is written as an integral over the entire

flow." Descriptions of nonlocal rheology also focus on the concept of granular fluidity (e.g. Bocquet et al., 2009; see review by Bouzid et al., 2015), which is the reciprocal of the viscosity μ as defined by, say, a $\mu(I)$ rheology that varies with the inertial number I. One approach involves envisioning the occurrence of plastic rearrangements over a characteristic length ξ during shear, where nonlocal behavior is then described by a diffusive term acting normal to shear, $\xi^2 \partial^2 \rho / \partial z^2$, which is added to a "local" expression of fluidity (Kamrin and Koval, 2012; Hennan and Kamrin, 2013, 2014). Importantly, these conceptualizations are centered on a physical (mechanical) interpretation of nonlocal behavior, which then points to the mathematics used.

Bibliography

[1] Allen, M. C. (2023) Probabilistic versus deterministic descriptions of bed load sediment transport: Clarifying the inherent variability in transport rates. MS thesis, Vanderbilt University, Nashville, Tennessee.

[2] Ancey, C. (2010) Stochastic modeling in sediment dynamics: Exner equation for planar bed incipient bed load transport conditions. *Journal of Geophysical Research – Earth Surface*, 115, F00A11, https://doi.org/10.1029/2009JF001260.

[3] Ancey, C., Bohorquez, P., and Heyman, J. (2015) Stochastic interpretation of the advection-diffusion equation and its relevance to bed load transport. *Journal of Geophysical Reserch – Earth Surface*, 120, 2529–2551, https://doi.org/10.1002/2014JF003421.

[4] Ancey, C., Davison, A., Böhm, T., Jodeau, M., and Frey, P. (2008) Entrainment and motion of coarse particles in a shallow water stream down a steep slope. *Journal of Fluid Mechanics*, 595, 83–114.

[5] Ancey, C. and Heyman, J. (2014) A microstructural approach to bed load transport: mean behaviour and fluctuations of particle transport rates. *Journal of Fluid Mechanics*, 744, 129–168.

[6] Ancey, C. and Pascal, I. (2020) Estimating mean bedload transport rates and their uncertainty. *Journal of Geophysical Research – Earth Surface*, 125, e2020JF005534, https://doi.org/10.1029/2020JF005534.

[7] Ancey, C. and Recking, A. (2023) Scaling behavior of bedload transport: what if Bagnold was right? *Earth-Science Reviews*, 246, 104571, https://doi.org/10.1016/j.earscirev.2023.104571.

[8] Andreotti, B. and Claudin, P. (2015) Aeolian and subaqueous bedforms in shear flows. *Philosophical Transactions of the Royal Society A*, 371, 20120364, http://dx.doi.org/10.1098/rsta.2012.0364.

[9] Ballio, F., Nikora, V., and Coleman, S. E. (2014) On the definition of solid discharge in hydro-environment research and applications. *Journal of Hydraulic Research*, 52, 173–184. doi:10.1080/00221686.2013.869267.

[10] Ballio, F., Pokrajac, D., Radice, A., and Sadabadi, S. A. (2018) Lagrangian and Eulerian description of bed load transport. *Journal of Geophysical Research – Earth Surface*, 123, 384–408, https://doi.org/10.1002/2016JF004087.

[11] Benson, D. A., R. Schumer, M. M. Meerschaert, and S. W. Wheatcraft (2001). Fractional dispersion, Lévy motion, and the MADE tracer tests. *Transport in Porous Media*, 42, 211–240.

[12] Benson, D. A., S. W. Wheatcraft, S. W., and M. M. Meerschaert, M. M. (2000) The fractional-order governing equation of Lévy motion. *Water Resources Research*, 36, 1413–1423.

[13] Bocquet, L., Colin, A., and Ajdari, A. (2009) Kinetic theory of plastic flow in soft glassy materials. *Physical Review Letters*, 103, 036001, doi: https://doi.org/10.1103/PhysRevLett.103.036001.

[14] Bohorquez, P., Papa, D. V., and Ancey, C. (2025) Multi-train roll waves, antidunes and bars in inclined flumes. *Earth-Science Reviews*, 271, 105308, doi.org/10.1016/j.earscirev.2025.105308.

[15] Bouzid, M., Izzet, A., Trulsson, M., Clément, E., Claudin, P., and Andreottia, B. (2015) Nonlocal rheology in dense granular flows: Revisiting the concept of fluidity. *The European Physical Journal E*, 38, 125, doi: 10.1140/epje/i2015-15125-1.

[16] Bridge, J. S. and Dominic, D. F. (1984) Bed load grain velocities and sediment transport rates. *Water Resources Research*, 20, 476–490.

[17] Chartrand, S. M. (2017) Pool-riffle dynamics in mountain streams: implications for maintenance, formation and equilibrium. PhD thesis, University of British Columbia, British Columbia, Canada.

[18] Charru, F., Andreotti, B., and Claudin, P. (2013) Sand ripples and dunes. *Annual Review of Fluid Mechanics*, 45, 469–493, doi: 10.1146/annurev-fluid-011212-140806.

[19] Coleman, S. E. and Nikora, V. I. (2009) Exner equation: A continuum approximation of a discrete granular system. *Water Resources Research*, 45, W09421, doi:10.1029/2008WR007604.

[20] Dhont, B. and Ancey, C. (2018) Are bedload transport pulses in gravel-bed rivers created by bar migration or sediment waves? *Geophysical Research Letters*, 45, 5501–5508.

[21] Doane, T. H. (2018) Theory and application of nonlocal hillslope sediment transport. PhD thesis, Vanderbilt University, Nashville, Tennessee.

[22] Doane, T. H., Furbish, D. J., Roering, J. J., Schumer, R., and Morgan, D. J. (2018) Nonlocal sediment transport on steep lateral moraines, eastern Sierra Nevada, California, USA. *Journal of Geophysical Research – Earth Surface*, 123, 187–208, https://doi.org/10.1002/2017JF004325.

[23] Doane, T. H., Roth, D. L., Roering, J. J., and Furbish, D. J. (2019) Compression and decay of hillslope topographic variance in Fourier wavenumber domain. Journal of *Geophysical Research – Earth Surface*, 124, 60–79, https://doi.org/10.1029/2018JF004724.

[24] Einstein, H. A. (1950) The bed-load function for sediment transportation in open channel flows. Technical Bulletin 1026, Soil Conservation Service, US Department of Agriculture, Washington, DC.

[25] Fan, N., Zhong, Q., Nie, R., and Liu, X. (2023) Interaction of various-sized particles in river flow. *Scientific Reports*, 13, 10503, https://doi.org/10.1038/s41598-023-37460-y.

[26] Fathel, S. L., Furbish, D. J. and Schmeeckle, M. W. (2015) Experimental evidence of statistical ensemble behavior in bed load sediment transport. *Journal of Geophysical Research – Earth Surface*, 120, 2298–2317, https://doi.org/10.1002/2015JF003552.

[27] Fazelpour, F. and Daniels, K. E. (2023) Controlling rheology via boundary conditions in dense granular flows. *Soft Matter*, 19, 2168–2175, doi:https://doi.org/10.1039/D2SM00683A.

[28] Foufoula-Georgiou, E., Ganti, V., and Dietrich, W. E. (2010) A nonlocal theory of sediment transport on hillslopes. *Journal of Geophysical Research – Earth Surface*, 115, F00A16, doi:10.1029/2009JF001280.

[29] Francalanci, S. and Solari, L. (2007) Gravitational effects on bed load transport at low Shields stress: Experimental observations. *Water Resources Research,* 43, W03424, doi:10.1029/2005WR004715.

[30] Furbish, D. J., Childs, E. M., Haff, P. K., and Schmeeckle, M. W. (2009a) Rain splash of soil grains as a stochastic advection–dispersion process, with implications for desert plant–soil interactions and land-surface evolution. *Journal of Geophysical Research – Earth Surface*, 114, F00A03, doi:10.1029/2009JF001265.

[31] Furbish, D. J. and Doane, T. H. (2021) Rarefied particle motions on hillslopes – Part 4: Philosophy. *Earth Surface Dynamics*, 9, 629–664, https://doi.org/10.5194/esurf-9-629-2021, 2021.

[32] Furbish, D. J., Fathel, S. L., and Schmeeckle, M. W. (2017a) Particle motions and bedload theory: The entrainment forms of the flux and the Exner equation. in: *Gravel-Bed Rivers: Processes and Disasters*, 1st Edn., edited by: Tsutsumi, D. and Laronne, J. B., John Wiley & Sons Ltd., https://onlinelibrary.wiley.com/doi/book/10.1002/9781118971437.

[33] Furbish, D. J., Fathel, S. L., Schmeeckle, M. W., Jerolmack, D. J., and Schumer, R. (2017b) The elements and richness of particle diffusion during sediment transport at small timescales. *Earth Surface Processes and Landforms*, 42, 214–237, doi: 10.1002/esp.4084.

[34] Furbish, D. J. and Haff, P. K. (2010) From divots to swales: Hillslope sediment transport across divers length scales. Journal of Geophysical Research – Earth Surface, 115, F03001, doi:10.1029/2009JF001576.

[35] Furbish, D. J., Haff, P. K., Roseberry, J. C., and Schmeeckle, M. W. (2012a) A probabilistic description of the bed load sediment flux: 1. Theory. *Journal of Geophysical Research – Earth Surface*, 117, F03031, doi:10.1029/2012JF002352.

[36] Furbish, D. J. and Roering, J. J. (2013) Sediment disentrainment and the concept of local versus nonlocal transport on hillslopes. *Journal of Geophysical Research – Earth Surface*, 118, 1–16, doi: 10.1002/jgrf.20071.

[37] Furbish, D. J., Roering, J. J., Doane, T. H., Roth, D. L., Williams, S. G. W., and Abbott, A. M. (2021a) Rarefied particle motions on hillslopes – Part 1: Theory. *Earth Surface Dynamics*, 9, 539–576, https://doi.org/10.5194/esurf-9-539-2021.

[38] Furbish, D. J., Williams, S. G.W., and Doane, T. H. (2021c) Rarefied particle motions on hillslopes – Part 3: Entropy. *Earth Surface Dynamics*, 9, 615–628, https://doi.org/10.5194/esurf-9-615-2021.

[39] Gomez, B. and Church, M. (1989) An assessment of bed load transport formulae for gravel bed rivers. *Water Resources Research*, 25, 1161–1186.

[40] Hancock, G. R. and Willgoose, G. R. (2021) Predicting gully erosion using landform evolution models: Insights from mining landforms. *Earth Surface Processes and Landforms*, 46, 3271–3290, https://doi.org/10.1002/esp.5234.

[41] Hassan, M. A., Chartrand S. M., Radić, V., Ferrer-Boix, C., Buckrell, E., and McDowell, C. (2022) Experiments on the sediment transport along pool-riffle unit. *Water Resources Research*, 58, e2022WR032796.

[42] Hassan, M. A. and M. Church, M. (2000) Experiments on surface structure and partial sediment transport on a gravel bed. *Water Resources Research*, 36, 1885–1895, doi: 10.1029/2000WR900055.

[43] Henann, D. L. and Kamrin, K. (2013) A predictive, size-dependent continuum model for dense granular flows. *Proceedings of the National Academy of Sciences*, 110, 6730–6735.

[44] Henann, D. L. and Kamrin, K. (2014) Continuum modeling of secondary rheology in dense granular materials. *Physical Review Letters*, 113, 178001, http://dx.doi.org/10.1103/PhysRevLett.113.178001.

[45] Heyman, J., Mettra, F., Ma, H., and Ancey, C. (2013) Statistics of bedload transport over steep slopes: Separation of time scales and collective motion. *Geophysical Research Letters*, 40, 128–133, https://doi.org/10.1029/2012gl054280.

[46] Kamrin, K. and Koval, G. (2012) Nonlocal constitutive relation for steady granular flow. *Physical Review Letters*, 108, 178301, doi: 10.1103/PhysRevLett.108.178301.

[47] Lajeunesse, E., Malverti, L., and Charru, F. (2010) Bed load transport in turbulent flow at the grain scale: experiments and modeling. Journal of Geophysical Research – Earth Surface, 115, F04001.

[48] Lee, D. B. and Jerolmack, D. (2018) Determining the scales of collective entrainment in collision-driven bed load. *Earth Surface Dynamics*, 6, 1089–1099, https://doi.org/10.5194/esurf-6-1089-2018.

[49] Li, Z., Oshtorjani, M. K., Chen, D., Zhang, Y., and Sun, H. (2023) Dynamics of dual-mode bedload transport with three-dimensional alternate bars migration in subcritical flow: Experiments and model analysis. *Journal of Geophysical Research – Earth Surface*, 128, e2022JF006882.

[50] Ma, H., Heyman, J., Fu, X., Mettra, F., Ancey, C., and Parker, G. (2014) Bed load transport over a broad range of timescales: Determination of three regimes of fluctuations. Journal of Geophysical Research – Earth Surface, 119, 2653–2673, doi: 10.1002/2014JF003308.

[51] Masteller, C. C. and Finnegan, N. J. (2017) Interplay between grain protrusion and sediment entrainment in an experimental flume. *Journal of Geophysical Research – Earth Surface*, 122, 274–289, doi:10.1002/2016JF003943.

[52] McGuire. L. A., Pelletier, J. D., Gómez, J. A., and Nearing, M. A. (2013) Controls on the spacing and geometry of rill networks on hillslopes: Rain splash detachment, initial hillslope roughness, and the competition between fluvial and colluvial transport. *Journal of Geophysical Research – Earth Surface*, 118, 241–256.

[53] Nakagawa, T. (2011) *Stochastic Processes with Applications to Reliability Theory*. Springer-Verlag, London.

[54] Nagakawa, H. and Tsujimoto, T. (1980) Sand bed instability due to bed-load motion. *Journal of the Hydraulics Division*, ASCE, 106, No. HY12.

[55] Nelson, J. M. (1990) The initial instability and finite-amplitude stability of alternate bars in straight channels. *Earth-Science Reviews*, 29, 97–115.

[56] Parker, G., Seminara, G., and Solari, L. (2003) Bed load at low Shields stress on arbitrarily sloping beds: Alternative entrainment formulation. *Water Resources Research*, 39, 1183, doi:10.1029/2001WR001253.

[57] Pierce, J. K. (2021) The stochastic movements of individual streambed grains. PhD thesis, University of British Columbia, British Columbia, Canada.

[58] Pierce, K., Hassan, M. A., and Ferreira, R. M. L. (2022) Probabilistic description of bedload fluxes from the aggregate dynamics of individual grains. *Earth Surface Dynamics*, 10, 817–832, https://doi.org/10.5194/esurf-10-817-2022.

[59] Pouliquen, O. and Forterre, Y. (2009) A non-local rheology for dense granular flows. *Philosophical Transactions of the Royal Society A*, 367, 5091–5107, http://doi.org/10.1098/rsta.2009.0171.

[60] Roseberry, J. C., Schmeeckle, M. W., and Furbish, D. J. (2012) A probabilistic description of the bed load sediment flux. 2. Particle activity and motions. *Journal of Geophysical Research – Earth Surface*, 117, F03032.

[61] Schumer, R., Benson, D. A., Meerschaert, M. M., and Baeumer, B. (2003) Fractal mobile/immobile solute transport. *Water Resources Research*, 39, 1296, doi:10.1029/2003WR002141.

[62] Schumer, R., Meerschaert, M. M. and Baeumer, B. (2009) Fractional advection–dispersion equations for modeling transport at the Earth surface. *Journal of Geophysical Research – Earth Surface*, 114, F00A07, https://doi.org/10.1029/2008JF001246.

[63] Seminara, G., Solari, L., and Parker, G. (2002) Bed load at low Shields stress on arbitrarily sloping beds: Failure of the Bagnold hypothesis. *Water Resources Research*, 38, 1249, doi:10.1029/2001WR000681.

[64] Singh, A., Fienberg, K., Jerolmack, D. J., Marr, J., and Foufoula-Georgiou, E. (2009) Experimental evidence for statistical scaling and intermittency in sediment transport rates. *Journal of Geophysical Research – Earth Surface*, 114, F01025, doi: 10.1029/2007JF000963.

[65] Smith, J. A., Hui, E., Steiner, M., Baeck, M. L., Krajewski, W. F., and Ntelekos, A. A. (2009) Variability of rainfall rate and raindrop size distributions in heavy rain. *Water Resources Research*, 45, W04430.

[66] Tang, Z., Brzinski, T. A., Shearer, M., and Daniels, K. E. (2018) Nonlocal rheology of dense granular flow in annular shear experiments. *Soft Matter*, 14, 3040–3048, https://doi.org/10.1039/C8SM00047F.

[67] Tsujimoto, T. (1978) Probabilistic model of the process of bed load transport and its application to mobile-bed problems. PhD thesis, Kyoto University, Japan.

[68] Uijlenhoet, R., Stricker, J. N. M, Torfs, P. J. J. F., and Creutin, J. D. (1999) Towards a stochastic model of rainfall for radar hydrology: Testing the Poisson homogeneity hypothesis. *Physics and Chemistry of the Earth*, Part B, 24, 747–755, doi:10.1016/S1464-1909(99)00076-3.

[69] Wiberg, P. L. and Smith, J. D. (1989) Model for calculating bedload transport of sediment. *Journal of Hydraulic Engineering*, 115, 101–123.

[70] Williams, S. G. W. and Furbish, D. J. (2021) Particle energy partitioning and transverse diffusion during rarefied travel on an experimental hillslope. *Earth Surface Dynamics*, 9, 701–721, https://doi.org/10.5194/esurf-9-701-2021.

[71] Wong, M., Parker, G., DeVries, P., Brown, T. M., and Burges, S. J. (2007) Experiments on dispersion of tracer stones under lower-regime plane-bed equilibrium bed load transport. *Water Resources Research*, 43, W03440, doi:10.1029/2006WR005172.

[72] Wu, Z., Furbish, D., and Foufoula-Georgiou, E. (2020) Generalization of hop distance-time scaling and particle velocity distributions via a two-regime formalism of bedload particle motions. *Water Resources Research*, 56, e2019WR025116, https://doi.org/10.1029/2019WR025116.

[73] Yager, E. M., Schmeeckle, M. W., and Badoux, A. (2018) Resistance is not futile: Grain resistance controls on observed critical Shields stress variations. *Journal of Geophysical Research – Earth Surface*, 123, 3308–3322, https://doi.org/10.1029/2018JF004817.

[74] Yannaros, N. (1994) Weibull renewal processes. *Annals of the Institute of Statistical Mathematics*, 46, 641–648.